Contrib Mineral Petrol (2000) 140: 296–315

Philippe Agard · Bruno Goffé · Jacques L. R. Touret
Olivier Vidal

Retrograde mineral and fluid evolution in high-pressure metapelites (Schistes lustrés unit, Western Alps)

Received: 19 October 1998 / Accepted: 19 July 2000

Abstract Fluid inclusions have been analysed in successive generations of syn-metamorphic segregations within low-grade, high-pressure, low-temperature (HP–LT) metapelites from the Western Alps. Fluid composition was then compared to mass transfer deduced from outcrop-scale retrograde mineral reactions. Two types of quartz segregations (veins) occur in the 'Schistes lustrés' unit: early blueschist-facies carpholite-bearing veins (BS) and retrograde greenschist-facies chlorite-bearing veins (GS). Fluid inclusions in both types of segregations are aqueous (no trace of dissolved gases such as CO_2, CH_4, N_2), with significant differences in density and composition (salinity). BS fluids are moderately saline fluids (average 9.1 wt% eq. NaCl) characterized by a chronological trend towards more dilute composition (from 15 down to 0 wt% eq. NaCl), whereas GS fluids have a very constant salinity of ~3.7 wt% eq. NaCl. Both types of inclusions were continuously reset to lower densities along the retrograde path, until a temperature of ~300 °C. Mass-balance calculations, together with fluid inclusion data, suggest that GS fluids result from the mixing between two fluid sources: one initial, early metamorphic, moderately saline HP fluid and a second nearly pure water fluid provided by the breakdown of carpholite. Estimates of the amount of water released by carpholite breakdown result in a dilution of the interstitial fluid phase (from 10 to 2.5–4 wt% eq. NaCl) consistent with the actual shift of the fluid composition. Alkali elements required for the formation of the GS chlorite + phengite assemblage after carpholite could be locally provided by HP phengite. This is taken as an indirect evidence that, during the generation of both BS and GS fluids, mixing with externally derived fluids may have been very limited. The location, amount and constant composition of the less saline GS fluids appear to be related to an interconnected porosity at the time of inclusion formation.

P. Agard (✉) · B. Goffé · J. L. R. Touret · O. Vidal
Laboratoire de Géologie de l'Ecole Normale Supérieure,
UMR 8532, CNRS, 24, rue Lhomond,
75231 Paris Cedex, France
e-mail: agard@geologie.ens.fr

Present address:
J. L. R. Touret
Department of Petrology, Vrije Universiteit,
De Boelelaan 1085, 1081 HV Amsterdam, The Netherlands

Editorial responsibility: W. Schreyer

Introduction

The nature and behaviour of fluids, as well as the fluid flow at depth, is of prime importance in almost all aspects of metamorphic petrology (e.g. Etheridge et al. 1983; Walther and Wood 1986; Ferry 1994; Rumble 1994; Jamtveit and Yardley 1997). In the case of subduction- or collision-related metamorphism, fluids influence small-scale rock mineral transformations (e.g. Austrheim 1986; Selverstone et al. 1991) as well as large-scale geodynamic processes (Fyfe et al. 1978; Reynolds and Lister, 1987; Bousquet et al. 1997; Henry et al. 1997) or element transfer between crust and mantle (e.g. Touret 1996). Besides direct observation of fluid remnants trapped in mineral inclusions, the composition and the role of the fluid phase can be approached by different techniques: stable isotopes (Rumble 1994), metamorphic reactions (Ferry 1994), mass balance estimates based on whole-rock compositions (Ague 1991) or models of fluid circulation during progressive metamorphism (Etheridge et al. 1983) or rock deformation (Oliver 1996).

In the case of high-pressure (HP) metamorphism associated with either oceanic subduction or continental collision, these different approaches have led to a marked controversy between two opposite models: (1) large-scale fluid infiltration of relatively homogeneous, externally derived fluids in an essentially open regional system (Bebout and Barton 1993; Giaramita and Sorensen 1994; Moree 1998); and (2) limited circulation of compositionally varied fluids, internally buffered by local mineral reactions (Philippot and Selverstone 1991).

The last case is generally accepted for alpine metamorphism (see e.g. Getty and Selverstone 1994; Barnicoat and Cartwright 1995; Henry et al. 1996). In both cases, a significant part of the models relies on the direct determination of the syn-metamorphic fluid phase composition by fluid inclusion studies. In this respect, much work has been done on fluids in eclogites (Selverstone et al. 1992; Andersen et al. 1993; Philippot and Scambelluri 1995; Philippot et al. 1995), but only few studies have concentrated on blueschist facies metapelites (Barr 1990; Küster and Stöckhert 1997). Yet metapelites undergoing blueschist (BS) facies metamorphism could carry significant amounts of mineral-bound volatiles from the surface down to metamorphic depths (Touret 1992; Bebout 1996). They are important to constrain element recycling during subduction, notably in accretionary prisms.

Alpine blueschist metapelite occurrences – mostly located in the Liguro-Piemontese Schistes Lustrés (SL) unit – represent a vast, central domain that stretches all along the Franco-Italian western Alps (Fig. 1; Lemoine et al. 1986; Deville et al. 1992). Isotopic measurements of Henry et al. (1996), based on an extensive sampling of veins and their wallrocks in the Fraiteve area (Fig. 1), showed no large-scale whole-rock isotopic shift, suggesting that the SL unit there probably behaved as a rock-buffered system.

In the light of this study, the SL metapelites appear particularly suited for the study of fluid–rock interactions because of the following:

1. The composition of the fluid phase is expected to reflect the rock mineralogical evolution if the system remained closed at the meter scale. In particular, the mineralogy of the veins in the study area is identical to that of the host rock (see below), suggesting that the fluid budget (from which the segregations formed) was closely controlled by in situ metamorphic reactions (Goffé et al. 1987; Philippot and Selverstone 1991; Cesare 1994).
2. The metamorphic history is consistent with a single alpine subduction-related (P, T) path (e.g. Michard et al. 1996).
3. The mineralogical evolution appears to be simple, yet chemically contrasted: the HP stage is typified by the highly hydrous, alkali-free blueschist (BS) facies index minerals ferro-magnesio-carpholite (Fe, Mg)$Al_2Si_2O_7(OH)_2$ and lawsonite $CaAl_2Si_2O_7(OH)_2$, respectively, whereas the subsequent greenschist (GS) facies retrogression is accompanied by the development of alkali-bearing minerals (mainly micas).
4. Syn-metamorphic quartz-rich segregations, whose abundance testifies to the importance of fluid–rock interactions, are created throughout the different stages of the tectono-metamorphic evolution.

The aim of the present study is to approach fluid composition and budget during retrograde metamorphism by a combined study of fluid inclusions and mass transfer. Firstly, we investigate the little documented blueschist facies fluid composition by differentiating syn-metamorphic vein generations and analysing fluid inclusions by microthermometry. Secondly, we characterize mass transfer that takes place concomitantly in the rock system as retrograde mineral reaction(s) proceed. Thirdly, we compare mass transfer and fluid composition characteristics and discuss their bearing on the fluid phase evolution during the retrograde metamorphic history.

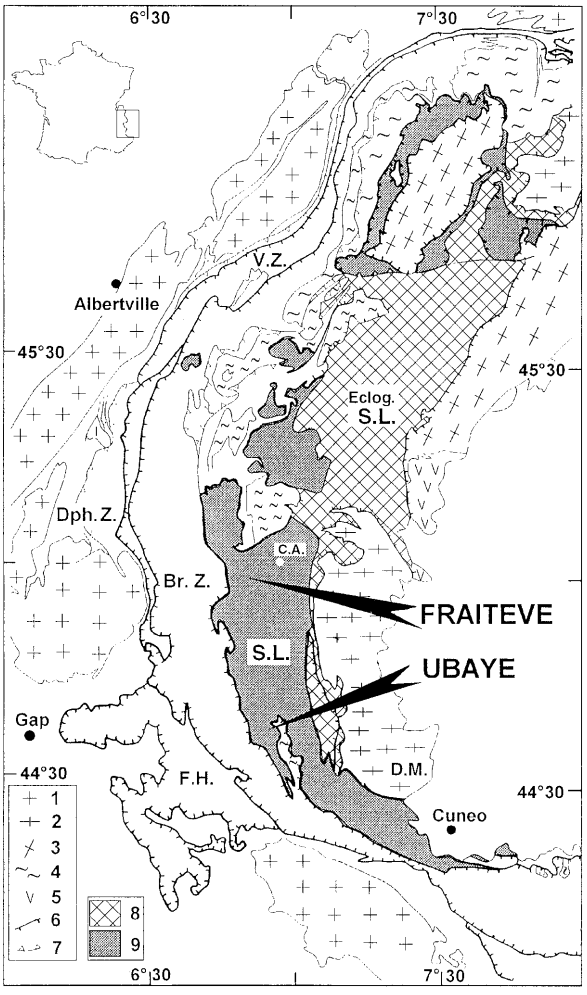

Fig. 1 Location of the Liguro-Piemontese units (*grey* and *criss-crossed*) in the Western Alps; sampling sites (Fraiteve, Ubaye) are indicated by *arrows*. *1* External crystalline massifs; *2* internal crystalline massifs; *3* Austro-Alpine zone: Sesia and Dent Blanche units; *4* basement units belonging to the Briançonnais zone; *5* Lanzo unit; *6* main tectonic contacts; *7* subsidiary tectonic contacts; *8* eclogitic Schistes Lustrés domain (*criss-crossed*); *9* non-eclogitic Schistes Lustrés domain (*grey*; after Pognante 1991). *Br.Z.* Briançonnais zone; *C.A.* Colle dell'Assietta; *D.M.* Dora Maira unit; *Dph.Z.* Dauphinois zone; *Eclog. S.L.* eclogitic Schistes Lustrés; *F.H.* Helminthoid flysch; *S.L.* non-eclogitic Schistes Lustrés; *V.Z.* Valais zone

Geological setting

Recent reviews of the geological setting of the Schistes Lustrés (SL) unit have been presented by Barfety et al.

(1995), Michard et al. (1996), Stampfli and Marchant (1997). The SL unit, which once belonged to the Liguro-piemontese domain derived from the alpine branch of the Thethys Ocean, represents a region 20 km wide, 200 km long and 10–15 km thick at present (Fig. 1). The SL unit essentially comprises calcschists and black-schists, of Malm to Senonian depositional age (Caron 1977; Barfety et al. 1995), with large interleaved metabasite bodies.

The SL unit is sandwiched between the low-grade, high-pressure Briançonnais unit to the west and the ultrahigh-pressure Dora Maira unit to the east (Goffé and Chopin 1986; Chopin et al. 1991; Fig. 1), both of which represent thinned European paleomargin units. The present setting is believed to result from the east- to southward subduction of the European and Liguro-piemontese domains under the Adria margin, followed by continental collision (Le Pichon et al. 1988; Platt et al. 1989).

The SL unit presents a regularly westward-dipping schistosity and a marked east–west stretching lineation (Caron 1977; Agard 1999). A first pervasive deformation, D1, took place under high-pressure blueschist (BS) facies conditions. It was responsible for kilometric isoclinal folds and associated sequence repetitions (Caron 1977; Tricart 1980). During exhumation, two distinct deformation events occurred (D2 and D3): they were classically regarded (Caron 1977; Lagabrielle 1987) as compressive events, but were recently described and reinterpreted as opposite vergence extensional movements (Agard et al. 2000b; south-east of the study area: Ballèvre et al. 1990; Philippot 1990). In particular, at small scale, there is abundant evidence that horizontal extension controlled the formation and location of many syn-metamorphic veins coeval with D2 and D3 events. Paleocene or early Eocene radiochronological ages obtained on phengite (50-35 Ma; Bocquet et al. 1974; Liewig 1981; Takeshita et al. 1994) probably relate to the D2 deformation event (Agard et al. 2000b). Further details pertaining to the D1–D3 tectonometamorphic events will be found below and in Agard et al. (2000b). The SL unit was finally affected by an ubiquitous brittle deformation episode.

Metamorphic evolution

Petrography

Across the Schistes Lustrés unit, HP–LT metamorphic conditions grade from blueschist facies conditions to eclogite facies conditions eastwards, close to the internal Dora Maira domain (Caby et al. 1978; Saliot et al. 1980; Goffé and Chopin 1986; Chopin et al. 1991; Pognante 1991; Agard 1999). We focused our study on the western part of the SL unit (Fraiteve, Ubaye; Fig. 1), where the HP assemblages are best preserved from the retrograde overprint. The widespread occurrence of lawsonite and the HP index mineral ferro-magnesio-carpholite (Goffé 1982; Chopin and Schreyer 1983; Goffé and Chopin 1986; Oberhänsli et al. 1995) in the metapelites, and of jadeite + quartz, glaucophane and lawsonite (Saliot et al. 1980) in rare metabasite lenses, points to BS facies conditions (Spear 1993). East of the study area (east of Colle dell'Assietta; Fig. 1) carpholite was replaced by chloritoid, which is consistent with the regional temperature increase (Vidal et al. 1992).

In the investigated metapelites, lawsonite and carpholite are encountered in both the massive rocks and in syn-metamorphic quartz-rich veins, which represent a significant fraction of any outcrop. Other ubiquitous minerals include calcite, which commonly makes up to 30–40% of the rocks in the calc-schist series, and accessory minerals such as rutile, hematite and tourmaline.

Lawsonite is particularly abundant in the calcium-rich metapelites (Sicard-Lochon 1987). In the segregations, light honey-coloured fibrous lawsonite crystals often reach 10 cm. However, lawsonite veins appear to have formed rather continuously from HP conditions down to medium pressure conditions (~4 kbar; Caron 1974), leading to late replacement of lawsonite by paragonite or phengite + calcite ± chlorite (Sicard-Lochon 1987). We therefore concentrated our study on carpholite-bearing segregations, which allow a more reliable discrimination between HP and retrograde segregations.

Carpholite is abundant in black-schist lithologies but was largely overprinted during the retrograde evolution by a mixture of phengite and ferromagnesian chlorite (as in the Valaisan 'Schistes lustrés'; Goffé and Bousquet 1997). Fresh carpholite may still be sampled in some HP syn-metamorphic segregations (sometimes together with high-pressure phengite, PhgA; Fig. 2), but in most cases it occurs as partial pseudomorphs filled with chlorite and phengite. Only ghost carpholite crystal shapes are visible in the adjacent schist.

The association chlorite + phengite is the typical retrograde assemblage in the SL metapelites, and will be hereafter referred to as the retrograde 'greenschist' (GS) facies assemblage for convenience. During the retrograde evolution (D2 and D3 deformation events), two phengite generations replacing carpholite (Phg1 and Phg2, respectively) were differentiated on the basis of habitus and microtexture (Agard et al. 2000a; Fig. 2). Phg1 is oriented along the D2 foliation, whereas Phg2 occurs as patchy crystals growing on isolated carpholite pseudomorphs. Their composition may be described by the structural formula $I_y[Si_{3+x}, Al_{1-x}][(Fe, Mg)_xAl_{2-x}]O_{10}(OH)_2$, where I refers to the interlayer site (mainly K^+, plus some Na^+ and NH_4^+; $y < 1$, usually). Later Phg2 shows both a lower interlayer and Si content (x_{Phg2}~3.2, y_{Phg2}~0.8) than Phg1 (x_{Phg1}~3.3, y_{Phg1}~0.9; Agard and Goffé 1998; Agard et al. 2000a; see below and Table 5).

Pressure–temperature (P–T) conditions

P–T conditions can be determined using recent thermodynamic data for metapelite mineralogy. A brief justification for the P–T path obtained for the Fraiteve

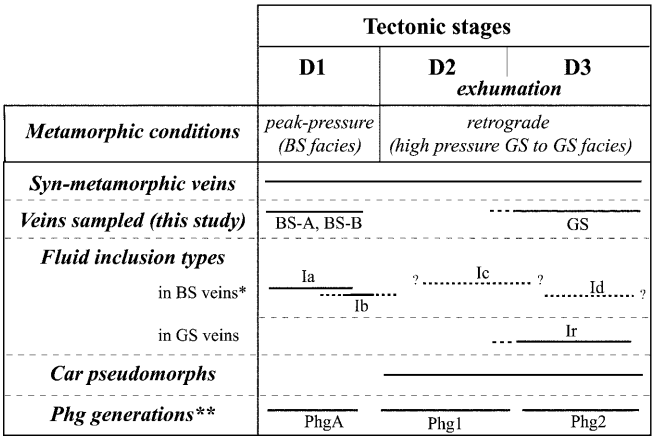

Fig. 2 Summary of the petrographic observations (segregation, fluid inclusion, pseudomorph and phengite characteristics) with respect to the tectono-metamorphic evolution from blueschist (*BS*) to greenschist (*GS*) facies conditions. *As discussed in "Fluid chronology in BS segregations"; **Agard et al. (2000a)

(and Ubaye) area is given below, but the reader is referred to Agard et al. (2000a) for full details. For the construction of the (P–T) grid (Fig. 3) using PTAX – a development of the Geocalc software (Berman and Perkins 1987) – the internally consistent data set of Berman (1988) has been complemented by consistent thermodynamic properties for magnesiocarpholite (Vidal et al. 1992) and phengite (Massonne 1995). Thermodynamic data used for magnesiochloritoid, obtained from Patrick and Berman (in Vidal and Theye 1996; Goffé and Bousquet 1997), are provisional. Mineral activities were calculated following Evans (1990) for epidote, Vidal et al. (1992) for chlorite, magnesiocarpholite, and magnesiochloritoid, and Massonne (1995) for phengite, on the basis of measured ferrocarpholite, chlorite and chloritoid compositions in schists and calcschists. Electron probe microanalysis (EPMA) was performed using Camebax and SX 50 (Cameca instruments; 15 kV, 10–20 nA beam conditions) at the University Pierre et Marie Curie, Paris. Standards used were Fe_2O_3 (Fe), $MnTiO_3$ (Ti), diopside (Mg, Si), orthoclase (K, Al), albite (Na), anorthite (Ca), and the analytical spot size diameter was ~2 μm.

Temperature constraints are given by chloritoid, which only occurs in the most ferrous rock compositions in the Fraiteve area (where $X_{Mg} = Mg/Mg + Fe$ ranges from 0.06 to 0.07; curve 3, Fig. 3), whereas it is present in all rock compositions 10 km eastward ($X_{Mg} = 0.11$ and T~400 °C at Colle dell'Assietta; curve 3′, Fig. 3). The geothermometer of Vidal et al. (1999), based on Fe/Mg partitioning in chlorite/chloritoid pairs, constrains maximum temperatures at ~380 °C (for the X_{Mg} values mentioned above, respectively; curves 4–4′, Fig. 3) for the chloritoid sampled in Fraiteve associated with chlorite of constant composition ($X_{Mg} = 0.36$). Temperature estimates derived from interlayer occupancy in phengite are comparable though slightly lower (~350 °C; Agard et al. 2000a).

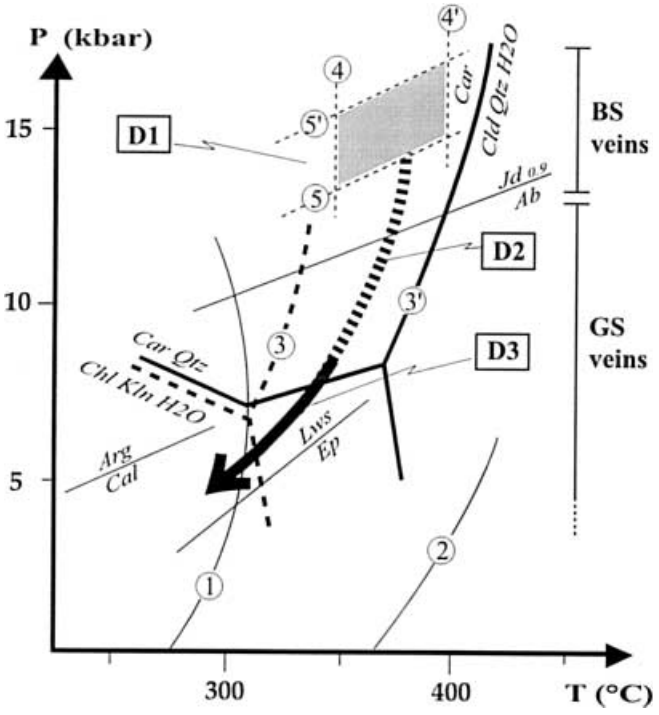

Fig. 3 P–T conditions determined for the Schistes Lustrés (*SL*) metapelites. The tectono-metamorphic evolution from blueschist (*BS*) to greenschist (*GS*) facies conditions is indicated by the *arrow* (*dashed* and *thick portions*: D2 and D3 deformation events, respectively; see Fig. 2 and text). Considered reactions and isopleths (abbreviations after Kretz 1983): *1* Kln + Qtz = Prl + W; *2* Prl = Ky + Qtz + W; *3-3′* Car = Cld + Qtz + W corresponding to $X^{car}_{Mg} = 0.31$ and 0.36 and $X^{ctd}_{Mg} = 0.06$ and 0.11 respectively; *4–4′* chloritoid geothermometer of Vidal et al. (1999); *5-5′* Car + Ce = Qtz + Chl + Mus + W corresponding to $Si^{4+} = 3.3$ and 3.4 in phengites (early PhgA; see Fig. 2 and Agard et al. 2000). *Other curves* Car–Qtz/Chl–Kln–H_2O: Chl + ln = Car + Qtz + (and its equivalent in the pyrophyllite field Car + Qtz = Chl + Prl + W); $Jd_{0.9}$ /Ab: Ab = $Jd_{0.9}$ + Qtz; Lws/Ep: Lws + Qtz = Prl + Zo + W (and its equivalent in the kaolinite field); Arg/Cal: aragonite–calcite

Peak pressure estimates are derived from phengite isopleths (e.g. Oberhänsli et al. 1995; curves 5–5′, Fig. 3) using compositions of phengite actually observed in Fraiteve and Ubaye. This method suggests that the peak of pressure reached 14–15 kbar during the HP stage (PhgA; Agard et al. 2000a). The compositions of Phg1 and Phg2 point to progressively decreasing high-pressure greenschist facies conditions, as the D2 and D3 deformation events take place (Fig. 3).

Estimated (*P*,*T*) conditions for the BS stage, ~14–15 kbar and 380 °C for Fraiteve and Ubaye, are in fair agreement with the appearance of ferrous rather than magnesian chloritoid (Vidal et al. 1992). These conditions also agree with the regional occurrence of lawsonite, glaucophane and nearly pure jadeite in metabasites (Saliot 1978; Evans 1990). During the decompressive path, neither epidote nor more magnesian chloritoid (curve 3′, Fig. 3) ever develop in metapelites. Additional constraints on the low-pressure conditions come from the breakdown of aragonite occurring at a temperature above 250–280 °C for pressure ~5–6 kbar (Gillet and

Goffé 1988; Liu and Yund 1993). The resulting decompressive P–T evolution is shown in Fig. 3.

Syn-metamorphic segregations

Several generations of syn-metamorphic veins can be recognized on the field (e.g. Fig. 4a). The genetic relationships between syn-metamorphic segregations, P–T conditions, and the deformation events are summarized in Fig. 2. Blueschist segregations contain quartz and relics of HP minerals, carpholite or lawsonite. Retrograde quartz ± chlorite greenschist segregations, showing no sign of former HP metamorphism, are related to the D2 or D3 deformation events. Late calcite, quartz, or quartz-albite bearing veins associated with brittle deformation, often showing 'en echelon' patterns (Fig. 4d), were not further considered in the present study.

HP segregations

Two types of blueschist facies segregations were recognized:

– BS-A segregations occur in metre-scale vein pods. They comprise patches of acicular carpholite crystals

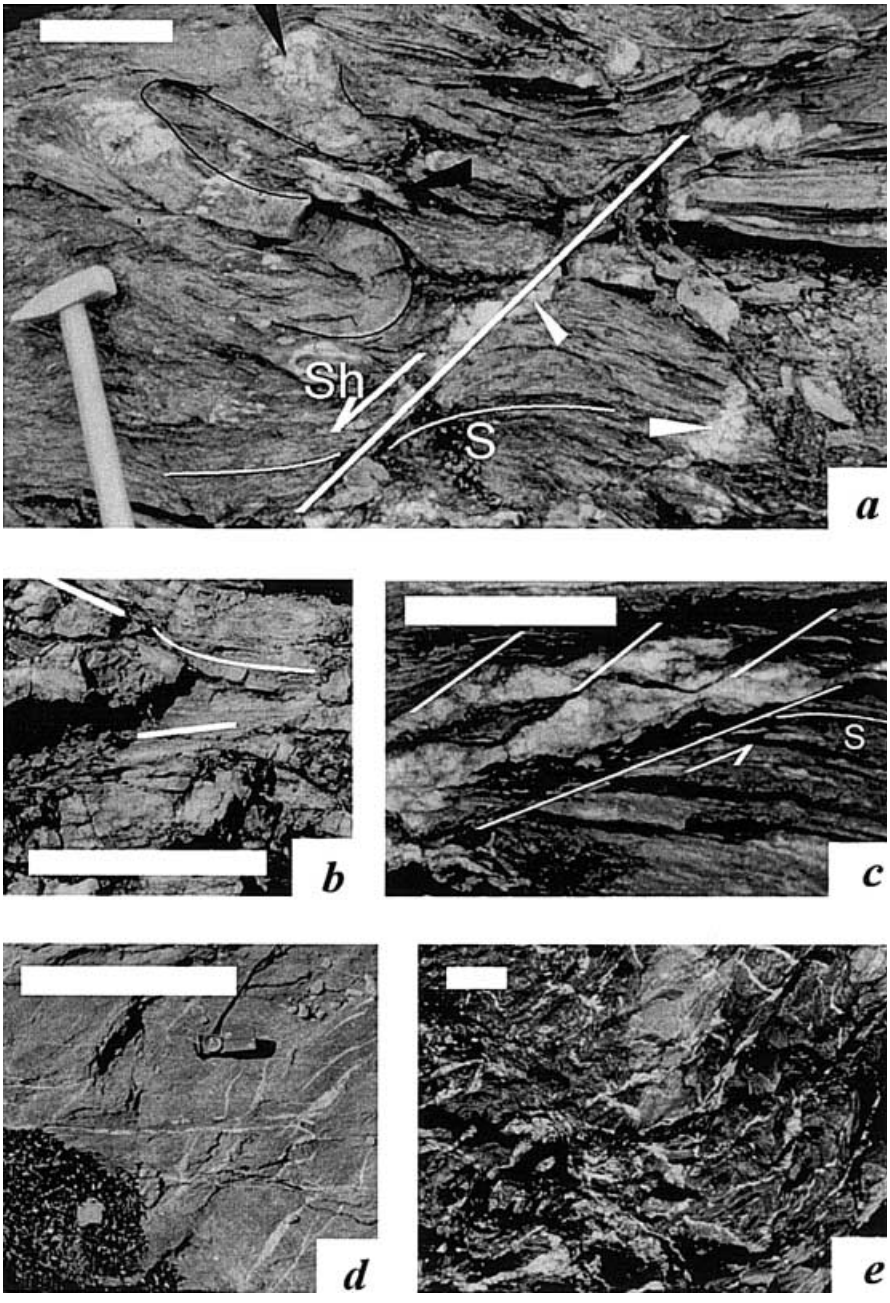

Fig. 4 Common features of syn-metamorphic segregations found in the Schistes Lustrés metapelites. *Scale bar* 20 cm. **a** Characteristic metre-scale outcrop of Schistes Lustrés metapelites. *S* Schistosity; *Sh* shear band; *black arrowheads* high-P carpholite-bearing blueschist facies (BS) segregations; *white arrowheads* greenschist facies (GS) segregations. Folds and highly deformed BS segregations (underlined by a *thin black line*) appear parallel to the schistosity planes away from the shear band. In contrast, GS segregations cut through the schistosity or occur within the shear band; and they clearly post-date BS segregations. **b** Blueschist BS-B segregation with stretched carpholite crystals parallel to the *white marks*. **c** Calcite–quartz GS veins within a small scale shear zone: evidences for syn- to post-D2 shearing (Fraiteve area); *white lines* underline small-scale shear bands; *S* schistosity. **d** Veinlets associated with the late brittle deformation phase. **e** Dense array of GS veins associated with D3 deformation

with variable orientations, sometimes normal to the walls.

– in contrast, BS-B segregations are very deformed, elongate or S-shaped, and subparallel to the present schistosity. These segregations contain elongate HP carpholite fibres, sometimes reaching 25 cm (Fig. 4b), where carpholite occurs intimately intergrown with quartz. Carpholite crystals of variable width generally have their [001] axis parallel to the *c*-axis of the surrounding quartz. In YZ thin sections, quartz–carpholite grain boundaries display characteristic scale invariant, fractal-like patterns (e.g. Fig. 8d; Mandelbrot 1977). When carpholite is destroyed by shallow alteration, the contours of quartz preserve this characteristic fractal shape, so that these BS-B segregations can be recognized easily in the field. At the thin section scale, fresh carpholite needles are found in low-strain domains where large, single quartz grains have been preserved from recrystallization. Wherever quartz subgrains are observed, the retrogression of the carpholite needles is complete.

Both BS-A and BS-B segregations formed during D1, but are interpreted to have formed in different microstructural sites. Based on outcrop scale estimates, carpholite-bearing syn-metamorphic segregations represented an important part of the total outcrop volume, up to 15–20 vol% in the case of Fraiteve.

Retrograde segregations

Retrograde carbonate–quartz–(chlorite) bearing segregations are the most conspicuous in the investigated area. These greenschist segregations, which are mostly extension veins (Ramsay and Huber 1983), are roughly elliptic in shape, 20 cm in length on average, discordant to the schistosity (Fig. 4c). Even in places of denser veining, the veins are generally not connected (Fig. 4e). At the thin section scale, quartz crystals are little deformed and preserve crack-seal patterns (Ramsay 1980). These quartz crystals often include chlorite aggregates characterized by a distinctive vermicular shape, but they never contain relics or pseudomorphs after carpholite. Most GS veins formed during D2 (Fig. 4a, c), some during D3 (Fig. 4e).

Composition of metamorphic fluids: fluid inclusion studies

The fact that most early blueschist segregations have been affected by a late retrograde overprint casts a fundamental doubt on the possibility to differentiate fluids in blueschist and greenschist veins by bulk crush-leach analysis (Banks and Yardley 1992). We therefore concentrated on the individual, non-destructive characterization of selected inclusions by microthermometry (e.g. Roedder 1984; Crawford and Hollister 1986; De Vivo and Frezzotti 1994). The complexity of the inclusion distribution in a single vein and the necessity of performing a sufficient number of measurements for each 'family' of inclusions evidently limit the possible number of studied localities. Two representative sites located at the front of the Schistes Lustrés unit were thus selected for sampling. The monotonous composition of the SL metapelites and the constancy of metamorphic assemblages suggest that the conclusions reached for the two sites studied in detail remain valid for all locations within the same metamorphic grade.

Sampling and analytical techniques

The two sampling sites, in the Ubaye valley and near mount Fraiteve, respectively (Fig. 1), meet a number of favourable conditions: they are representative of the whole investigated area, comprise only metapelites as host rock, permit differentiation of BS- and GS-type segregations, and were little affected by late brittle deformation. Sampling concerned three categories of segregations: blueschist BS-A and BS-B segregations formed during D1, and greenschist GS segregations formed during D3 (Fig. 2 and Table 1).

All segregations within a given category have more or less the same types and abundances of inclusions: BS-A segregations are usually quite transparent, displaying few inclusions, whereas GS segregations frequently contain numerous trails, BS-B segregations being intermediate.

Microthermometry was performed with a Linkam THMS 600 heating–freezing stage (Shepherd 1985) on 150-μm-thick, double-polished thin section samples. Temperatures measured on two-phase inclusions are the temperature of melting (Tm), which is related to the concentration of dissolved salts in the fluid phase, and the temperature of homogenization (Th; homogenization into the liquid phase). The temperature of eutectic melting, which gives insights into the nature of the dissolved species, could not always be determined with accuracy. These temperature measurements are considered reproducible within 0.2 °C for Tm, and 0.5–1 °C for Th

Table 1 List of the syn-metamorphic quartz segregations studied: sample characteristics and fluid inclusion populations analysed by microthermometry (see also Figs. 2 and 5)

Sample	Location	Tectonics	Mineralogy	Segregation type	F.I. types
1	Fraiteve	D1(+D2/D3)	(Carpholite)-late micas	BS (B) cross-cut by late trails	Id
2a	Fraiteve	D1	Carpholite	BS (B)	Ia, Ic
2b	Fraiteve	D1	Carpholite	BS (A)	Ia
3	Fraiteve	D1(+D2/D3)	(Carpholite)-late micas	BS (B) cross-cut by late trails	Ic, Id
4	Ubaye	D1	Carpholite	BS (B)	Ia, Ic
5	Ubaye	D1	Carpholite	BS (B)	Ia, Ib, Ic, Id
6	Fraiteve	(D2-)D3	Chlorite	GS (C)	Ir
7	Fraiteve	(D2-)D3	Chlorite	GS (C)	Ir

(Shepherd 1985; Belkin 1994). In conjunction with the thermometric data, micro Raman analysis (VU, Amsterdam) and infrared laser ablation-coupled ICPMS analysis (ULB, Brussels) were also performed on selected individual inclusions.

Fluid inclusion types

Fluid inclusions are generally 5–20 μm long, mostly two-phase (liquid + vapour) at room temperature (Fig. 5d, f). In carpholite-bearing quartz, apparent daughter minerals resembling halite can be observed. This was, however, not confirmed by SEM observations, which showed that these features did correspond to needles of carpholite spearing through the quartz grain.

Fluids are essentially aqueous, with vapour bubbles of varying sizes. Unlike many other studies in comparable settings (e.g. Andersen et al. 1993; Mullis et al. 1994), no gaseous fluids (i.e. N_2, CH_4, etc.) could be detected by micro-Raman analysis of large vapour bubbles. Similarly, no clathrates were detected by microthermometry. Tests with the crushing stage (Al-Khatib and Touret 1973) show that only a few bubbles formed in a limited number of cases, the BS-A quartzes showing the largest size of bubbles. Some volatiles may thus be present but in too small an amount to be detected by microthermometry.

Although the density of the fluid inclusions is likely to have been considerably modified (depending on the creep strength of the host mineral; e.g. Roedder 1984; Kuster and Stoekhert 1997), the inefficacy of diffusional processes in quartz at relatively low temperatures (< 400 °C; Sterner et al. 1995) suggest that fluid inclusions behaved as closed systems (i.e. retained their initial composition).

Some additional constraints come from fluid inclusions trapped in carpholite (Fig. 5c). These inclusions are numerous, lengthy, stretched and sometimes partly necked-down (e.g. Gratier and Jenatton 1984; Touret 1992). The long axis of the fluid inclusions is often parallel to the [001] axis of carpholite (Fig. 5c), an observation that suggests that these inclusions were trapped during the crystallization of carpholite under high-pressure conditions.

Fluid chronology in BS segregations

In quartz grains from blueschist BS-A segregations, the earliest fluids are found in isolated inclusions that occur in little deformed quartz grains containing large, fresh carpholite crystals. In these quartz grains, fluid inclusions are generally extremely rare.

Blueschist BS-B quartz grains display tiny needles of carpholite as well as arrays of inclusions (Fig. 5a). Simple textural criteria (Touret 1981) allow for a clear morphological distinction between successive inclusion generations. Four categories were recognized ([Ia] to [Id]; Fig. 5b), based on the following criteria.

– In quartz grains which escaped recrystallization, inclusions of all sizes are scattered in a random array ([Ia] inclusions). Because they are located in a single quartz grain together with fresh carpholite needles, they are regarded as HP inclusions coeval with the crystallization of carpholite. Inclusions exceeding ~30 μm (dark patches on Fig. 5a, arrows) are often empty and show highly irregular shapes with, sometimes, radiating healed fractures underlined by small 'satellite' inclusions. Many isolated inclusions show evidence of stretching of the inclusion walls (Fig. 5d).

– Clusters of tiny inclusions ([Ic] inclusions, Fig. 5e) are located in subgrain domains of the large BS-B quartz grains. These subgrains contain both fresh and partially retrogressed carpholite needles.

– Inclusion trails occur in quartz grains still containing some fresh carpholite crystals among largely retrogressed ones. A small number of these trails (Fig. 5f) represent healed fractures outlined by tiny carpholite needles: such [Ib] inclusions contain a needle or are adjacent to a needle of carpholite. On the other hand, most healed fractures are marked by inclusion trails ([Id] inclusions) that cross-cut the entire quartz grain(s) (Fig. 5a, b) and are located close to retrogressed carpholite needles. These latter trails are abundant in some samples (see samples 1, 3; Table 1).

The [Ib] inclusions clearly post-date the isolated [Ia] inclusions, but since both co-exist with carpholite needles, they are believed to have formed during high-pressure conditions. The timing of formation of the cluster [Ic] inclusions is more speculative because it cannot be ascertained that these inclusions were sealed at HP conditions. This point will be discussed below in the light of microthermometric measurements. Late [Id] trails cross-cutting the quartz grains resemble and are interpreted as retrograde trails (Fig. 2).

Only one category of fluid inclusions ([Ir]) was found in retrograde GS segregations. These inclusions usually form planar trails of two-phase inclusions (Fig. 5g). They are small, rarely exceeding 15 μm, and have a regular elliptic or negative crystal shape. Stretching of these inclusions is less conspicuous than for the HP ones. Some fluid inclusion trails record crack-seal growth: parallel, planar trails are disposed perpendicular to the X stretching direction (Ramsay 1980).

Microthermometric results

Final melting (Tm) and homogenization (Th) temperatures were measured for some 150 inclusions. An overview of the results is presented in Fig. 6. All inclusions are essentially aqueous. Initial melting temperatures fall in the range −30–20 °C (mean: −23.6 °C, 2σ: 1.5), i.e. somewhat below the eutectic temperature for the system H_2O–NaCl (~−21 °C; Roedder 1984; Crawford and Hollister 1986). This indicates that fluid composition is not always pure NaCl, but Tm can still conveniently be

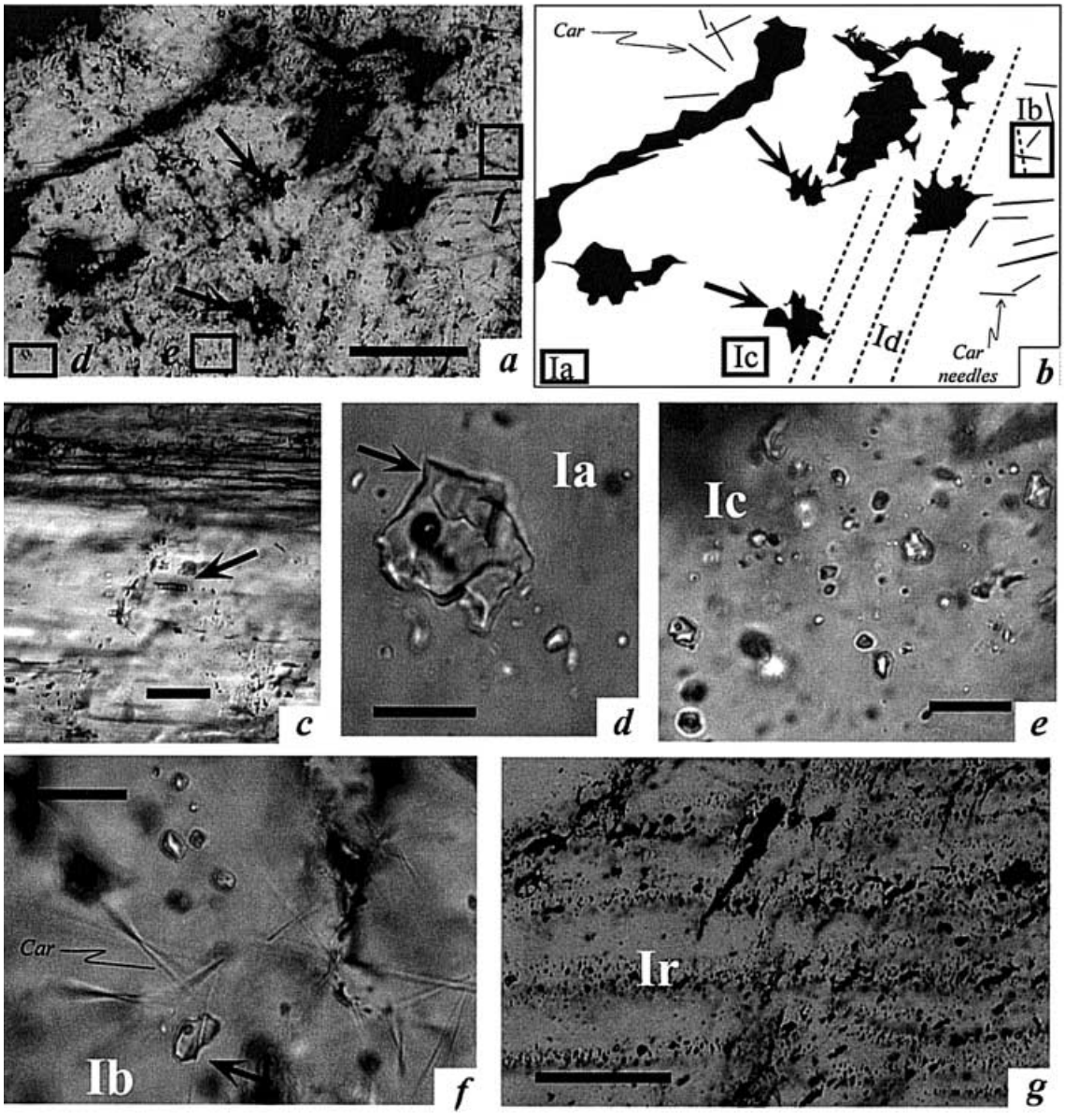

Fig. 5 Fluid inclusions types. Main features of the fluid inclusions from the blueschist (BS) and the greenschist (GS) segregations. *Scale bar* 20 μm except **a** and **g**, where *scale bar* 100 μm. **a** Typical aspect of the fluid inclusion array in quartz from a blueschist BS-B segregation (sample 5). Note the numerous decrepitated inclusions (dark patches, *thick arrows*). Carpholite needles, which are too thin to be unequivocally recognized here, are best seen on the *right-hand side* of this large-scale photograph. An interpretative sketch of this fluid inclusion population is drawn in **b**. Enlargements, which refer to **d–f**, correspond to [Ia], [Ic] and [Ib] inclusion types, respectively. **b** Interpretative sketch after **a** showing the successive generations of inclusions [Ia] to [Id] (see corresponding enlargements), and the position of the tiny carpholite (Car) needles. **c** Fluid inclusions trapped in carpholite (*sample 2b*; black diamonds in Fig. 6a). The central inclusion (*arrow*) is oriented and stretched along the [001] axis of carpholite. **d** Isolated [Ia] fluid inclusions showing incipient reequilibration (*arrow*). **e** Cluster of [Ic] inclusions. **f** Trails of [Ib] fluid inclusions coexisting with carpholite needles (Car). **g** Typical aspect of the [Ir] fluid inclusion trails in a GS segregation

expressed in wt% NaCl eq. (Roedder 1984), either graphically from the low-temperature phase diagram of the system H_2O–NaCl or from the analytical expression (Belkin 1994):

$$S = 1.78 * T_m - 0.0442 * T_m^2 + 0.000557 * T_m^3$$

Microthermometric results evidence moderate concentrations of salts (< 15 wt% eq. NaCl), but marked differences exist between blueschist and greenschist fluid inclusions. Bulk data, expressed in a Th–Tm diagram, point to GS fluids (empty circles, Fig. 6, above) with relatively constant Tm but Th variations, whereas BS fluids plot roughly parallel to the Tm axis (relatively constant Th, variable Tm; except for the [Id] inclusions). In other words, GS fluids are compositionally homogeneous (average 3.7 wt% eq. NaCl), whereas BS fluids are of relatively constant density but variable chemical composition (between 0 and 15 wt% eq. NaCl, with an

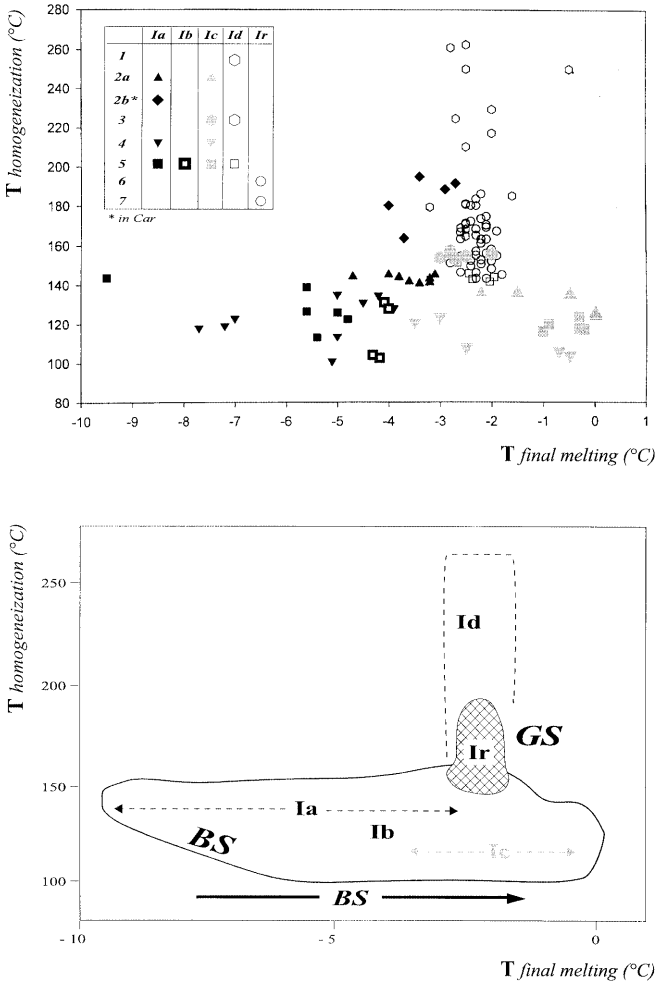

Fig. 6 *Above* Overview of the preliminary *Th*/*Tm* fluid inclusion data (*plain black*, *black and white*, *grey*, and *empty symbols* for [Ia], [Ib], [Ic] and [Id] inclusions, respectively; see *inset*). *Below* Interpretative diagram. Note the very different pattern for blueschist (*BS*) and greenschist (*GS*) inclusions: inclusions from BS segregations plot almost parallel to the horizontal *Tm* axis, and show decreasing *Tm* values with time ([Ia], [Ib], and then [Ic], as underlined by the *arrow*; see text for explanation) – except for the late, cross-cutting [Id] inclusions. In contrast, GS [Ir] inclusions plot over a limited range of *Tm* values comparable to that of [Id] inclusions

average composition slightly above 9 wt%). Fluid inclusions in carpholite (sample 2b, Fig. 6, above) differ slightly in density from inclusions in quartz, but have a similar average Tm. The salinity of these inclusions is also very close to the average salinity recorded in BS inclusions from the neighbouring quartz (sample 2a, Fig. 6).

Among fluid inclusions from BS segregations, reliable HP inclusions ([Ia] and [Ib], black symbols; Fig. 6, above) have higher salt concentrations (~15-5 wt% eq. NaCl) than [Ic] inclusions (grey symbols: 6-0 wt% eq. NaCl). Although only a few [Ib] inclusions could be measured, they fall in the lower range of salinities documented by the HP inclusions (~6.5 wt% eq. NaCl). Because of the chronological relationships between the fluid inclusions ([Ia], [Ib] and then [Ic]), these data suggest the existence of a salinity decrease with time in the fluid phase sampled by the BS segregations (Fig. 6, below). In particular, some [Ic] inclusions are less saline (almost pure H_2O) than most GS [Ir] inclusions and [Id] inclusions, which show similar salinity values.

Interpretation of the FI data

Representative fluid isochores, shown in Fig. 7, encompass the range of Tm and Th values. They define a narrow band that intersects the P–T path at pressure conditions (2–6 kbar) inconsistent with metamorphic pressures deduced from mineral equilibria, either for the high pressure or for the retrograde inclusions. This feature appears characteristic of HP–LT rocks (e.g. Touret 1992; Küster and Stöckhert 1997). Even the fluid in primary BS inclusions that shows no apparent sign of stretching or volume change has been reset to much lower densities (Fig. 7).

The experiments of Vityk et al. (1994) suggest that, at 300 °C, 20–30 μm size inclusions can only withstand an

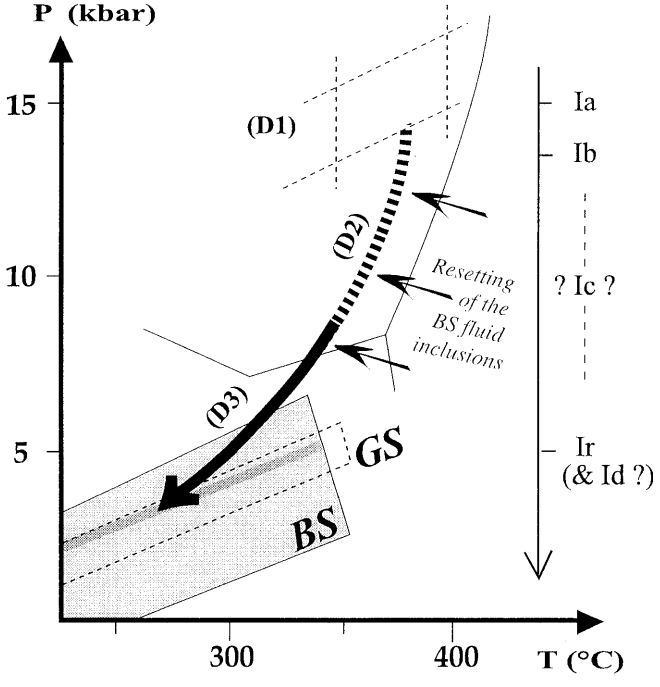

Fig. 7 Schematic diagram illustrating the entrapment and resetting history of the blueschist (*BS*) and greenschist (*GS*) facies fluid inclusions throughout the tectono-metamorphic evolution ([Ia] through [Ir]: fluid inclusion types; see text). The P–T path featured by the *arrow* is the same as in Fig. 3. The range of isochores inferred from microthermometry data for the BS and GS inclusions is represented by the *large grey area* and the *smaller dotted area*, respectively (*thick grey line*: average isochore for the BS inclusions). Maximum trapping P–T conditions for BS inclusions ([Ia], [Ib] and possibly [Ic]; see text), as determined through mineral equilibria (~14 kbar, 380 °C), contrast with the range of P–T conditions encompassed by fluid inclusion isochores

internal overpressure of ~2 kbar: larger overpressures lead to rupture. In contrast, the model of Küster and Stöckhert (1997) predicts continuous adaptation of the inclusion volume by creep of the host quartz at T > 300 °C for natural loading rates ($\sim 10^{-15}$ s^{-1}, which, as they point out, significantly differ from the rates used by Vityk et al. 1994).

Because temperature conditions during D1 and D2 exceed 300 °C (Fig. 7), it is suggested that differential pressure did not build up during exhumation and that fluid densities were continuously reset down to at least 3–4 kbar. Indeed, fluid isochores for the BS inclusions intersect the P–T path at ~300 °C and 3–4 kbar (Fig. 7), in agreement with the predictions of Küster and Stöckhert (1997). Some inclusions ([Ia] > 30 μm), however, show diagnostic decrepitation features (Touret 1977; Roedder 1984). This behaviour may be due to a size dependence of the adaptation by creep, which was not discussed in the model by Küster and Stöckhert (1997).

The trend in fluid salinity indicates a progressive dilution as P–T conditions evolve from BS to GS facies conditions (Fig. 6, below), which suggests the addition of less saline fluids during the retrograde evolution. On the other hand, GS fluid composition appears to be remarkably uniform (Fig. 6, below). To which extent these fluid composition characteristics relate to the in situ retrograde mineralogical evolution is the question addressed below. In the following section, we investigate the element transfer taking place during the retrograde mineral evolution, in particular during the breakdown of carpholite, which is the most important retrograde reaction occurring in metapelites.

Mineral reactions and mass transfer during vein formation

Methodology

As previously discussed, the carpholite + quartz assemblage found in relic blueschist segregations is the most reliable indicator of BS facies conditions in the metapelites. In contrast to the prograde evolution, mass balance calculations from the retrograde evolution are possible because the reaction textures and volume proportions of the mineral products chlorite and phengite are preserved.

The reaction carpholite → chlorite + phengite was investigated for blueschist segregations where the initial shape and volume of the carpholite crystals are still discernable (Fig. 8a, b). It is possible, in areas selected after careful optical microscope observations, to determine the volume change related to this reaction (Fig. $8b_1$) and the relative proportions of the reaction products (Fig. $8b_2$, b_3). Contours of the mineral phases were drawn, in part using SEM images to precisely control the interfaces. Scanned microphotographs or sketches were then used to determine the areas by image analysis (selected areas were ~500 × 500 μm on average).

Calculation of the amount of exchanged species was made following the method of Gresens (1967). The breakdown reaction of mineral A (carpholite) into reaction products B (chlorite) and C (mica) can be written :

$$A + \sum_{i=1,n} Xi \rightarrow v_B \cdot B + v_C \cdot C \ ,$$

where Xi corresponds to the amount of component i exchanged during the reaction, and v_B and v_C are the relative proportions of products. Area measurements allow estimation of the relative proportions of the product (i.e. $v_B/[v_B + v_C]$), and the overall volume change. As a first approximation, this overall volume change associated with the reaction is assumed to correspond to the volume of dissolved or precipitated quartz. The above equation was balanced by mineral compositions (A, B, C) actually measured by EMPA (CAM, Univ. PM Curie, Paris).

Mass balance constraints on carpholite breakdown

Area measurements for six samples coming from the two selected sites (Fraiteve and Ubaye) are shown in Table 2. For each sample, several carpholite pseudomorphs were measured (nine on average), either parallel or perpendicular to the (001) plane of carpholite (Table 2). The results are characterized by large 2σ values, but are remarkably coherent: there is more phengite than chlorite (~70 vs 30 vol%, on average) involved in carpholite pseudomorphs, and volume changes are always small and positive (~6.5 vol% on average). Several examples of carpholite pseudomorphs (Fig. 8b–f) with their corresponding area estimates (Table 2) illustrate this point.

In order to calculate the proportions of elements involved in the breakdown reaction, mean mineral compositions of A, B and C (out of five EPMA analyses) were considered for each sample. The balanced reactions obtained for the six different samples, using the volume change and the relative proportion of the products determined above (Table 2), are given in Table 3. These data show that, for each sample, the breakdown of carpholite into chlorite + phengite (Phg2) involves a consumption of alkali, and a coeval release of water and bivalent ferromagnesian elements. It is seen that the reaction is almost iso-aluminium.

Different sources of uncertainties contribute to errors in the mass balance estimates: (1) inaccuracy of EPMA analyses, (2) attribution and contouring of the mineral products, (3) estimation of the initial volume of carpholite, (4) representativity of the sections (i.e. the 3D problem), and (5) accuracy of image analysis. The first and the last factors are considered negligible (~1–2%), the second one was checked to be < 5%. The fourth source of uncertainty is large (2σ values for different orientations suggest that estimates are reliable within ~30%), but this problem is partly solved by the number of measurements ($n = 53$).

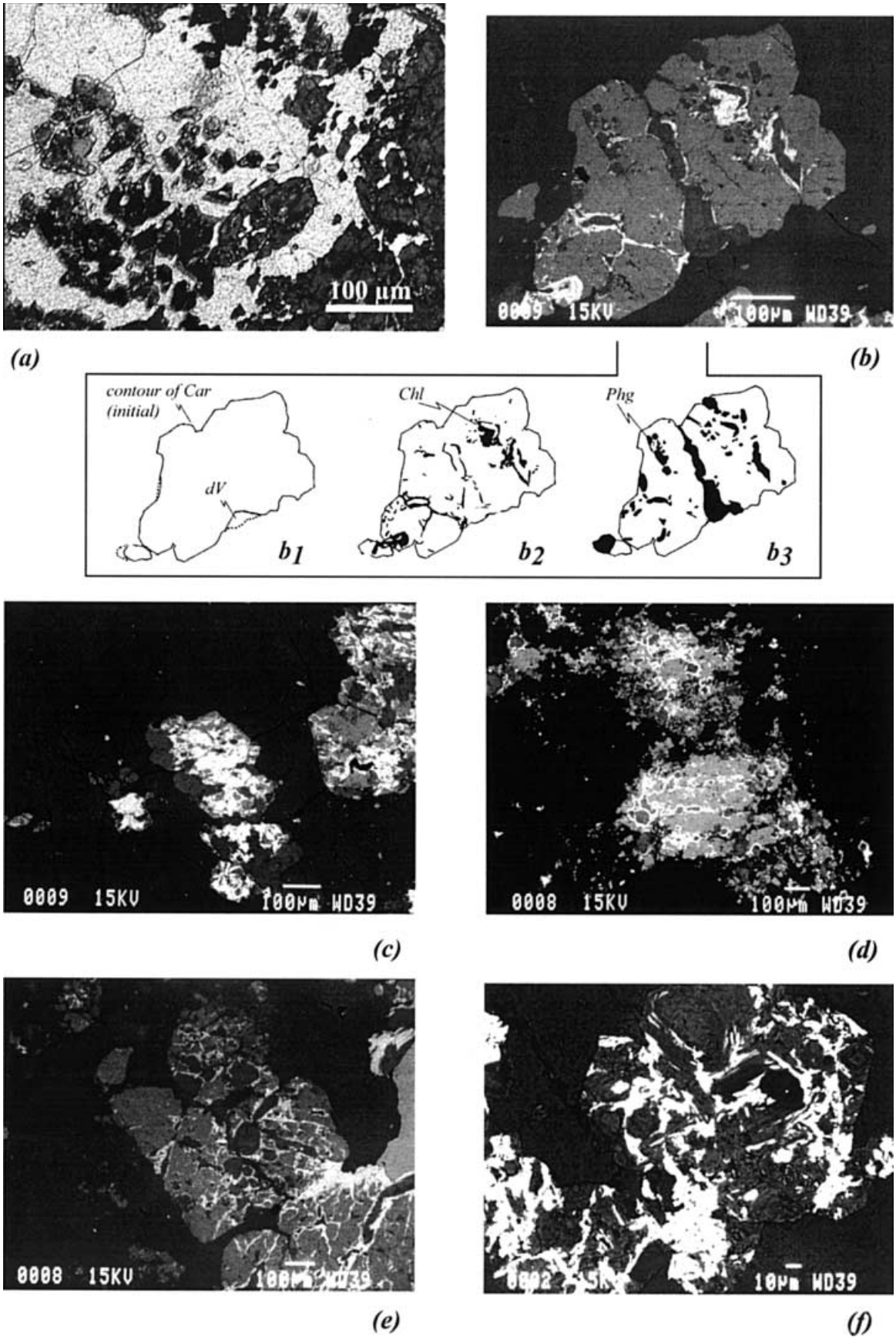
100 µm
0009 15KV 100µm WD39
(a)
(b)
contour of Car (initial)
dV
Chl
Phg
b1
b2
b3
0009 15KV 100µm WD39
0008 15KV 100µm WD39
(c)
(d)
0008 15KV 100µm WD39
10µm WD39
(e)
(f)

◄

Fig. 8 Characteristic features of quartz-hosted carpholite pseudomorphs [all sections parallel to the (001) plane of carpholite]. Area measurements for **b, c, e, f** are given in Table 2. **a** Microphotograph of fresh carpholite crystals (*dark*) dispersed in quartz (*white*; cross-polar light). **b** Scanning electron microscopy (SEM) image of a partial carpholite pseudomorph in quartz (sample β, Table 2). Discernable phases, from light to dark (in order of decreasing molar mass): chlorite, carpholite, phengite, and quartz (host). Related sketches: (b_1) contour of the initial carpholite crystal (*Car* continuous line) and volume increase (*dV* dashed line); (b_2) area measurement for chlorite, *outlined in black* (*Chl*); (b_3) area measurement for phengite, *outlined in black* (*Phg* see text). **c** SEM image of another pseudomorph showing a somewhat higher Chl/Phg ratio and a stronger overprint (sample χ, Table 2). **d** SEM image showing the characteristic fractal shape of carpholite pseudomorphs (see text). In this case, the overall volume change cannot be determined with accuracy. **e** SEM image illustrating the problem of connectivity between carpholite crystals and the difficulty to assess correctly the reaction products to either one of the adjacent crystals. Except for this sample (sample ε, Table 2), the study of such pseudomorphs has been discarded. **f** SEM close-up view of a largely retrogressed carpholite pseudomorph where initial contours are still discernable (sample ϕ, Table 2)

Uncertainties on the bulk volume change (point 3) are of the order of 40–50%. Element mobility was consequently plotted as a function of the volume factor, Fv (Fv = Vproducts/Vreactants; Gresens 1967), to help fine tune the mass balance calculations. Figure 9a shows that the reaction (for sample COA) is exactly iso-aluminium when Fv ~1.08, that is for a volume change of 7.9 vol% (arrow, Fig. 9a). This value compares well with the measured average value of 9.7 vol% (Table 2).

Since the greatest source of uncertainty comes from the volume change estimates, the carpholite breakdown reaction was nevertheless recast so that $\Delta Al = 0$, by adjusting the volume factor (case no. 3, Table 3) rather than the mineral proportions (case no. 2, Table 3). The following mean stoichiometric coefficients for the breakdown reaction are obtained (with Alk = Σ(Na,K) and R = Σ(Fe, Mn, Mg):

$$6.64\ \mathrm{Car} + 1.73\ \mathrm{Qtz} + 3.05\ \mathrm{Alk^+} + 0.81\ \mathrm{H^+} = \mathrm{Chl} + 3.82\ \mathrm{Phg2} + 6.0\ \mathrm{H_2O} + 1.93\ \mathrm{R^{2+}} + 0.02\ \mathrm{SiO_{2aq}} \quad (1)$$

Several points can be outlined.

1. Water is released in great quantities: reaction (1) is an obvious source for GS fluids.
2. The amount of alkali and ferromagnesian elements exchanged during the retrogression of carpholite is large.
3. Alkali availability is expected to be a key parameter. Indeed, as long as quartz-hosting carpholite is not recrystallized into subgrains, carpholite crystals remain completely protected from retrogression (i.e. from the access of alkali elements, which could have driven retrograde reactions).
4. Not all silicon provided by the dissolved quartz is needed to balance the reaction. Hence, some silicon is generally released, probably as amorphous silica (SiO_{2aq}, Table 3; except for sample RFB).

Table 2 Area measurements after carpholite pseudomorphs (→ Chl + Phg2) from six different blueschist segregations (n = 53) – all samples from Fraiteve, except GV from Ubaye (Fig. 1). *%Chl* Volume proportions of chlorite with respect to the chlorite + phengite (Phg2) assemblage; *%dV* volume change; *Or* orientation of the thin section with respect to the [001] axis of carpholite. β, χ, ε, ϕ area measurements corresponding to Fig 9b, c, e, f, respectively

GV (n = 7)			FBA (n = 11)			TPX (n = 6)			COA (n = 11)			Jacq (n = 10)			RFB (n = 8)		
%Chl	%dV	Or	%Chl	%dV	Or	%Chl	%dV	Or	%Chl	%dV	Or	%Chl	%dV	Or	%Chl	%dV	Or
25.5	4.7	a	27.3	10.5	a	23.1	4.6	b	25.3	7.7	a	20.1	12.4	a	19.5	0.0	a
29.8	8.6	a	30.8	3.2	b(χ)	37.7	15.0	a	32.1	10.0	a(β)	7.8	28.4	a	26.8	0.0	a (ϕ)
31.4	5.3	a	42.2	8.7	a	38.3	13.6	a	31.1	4.9	b	45.5	4.8	a	15.8	0.0	a
40.6	0.0	b	44.3	0.0	b	17.8	0.0	a	16.6	21.4	a	44.5	3.1	a	13.4	2.3	a
45.6	11.3	a	22.7	1.3	a	36.9	19.9	a	43.7	1.3	b	39.6	5.3	a	19.5	0.0	a
28.7	3.2	a	18.9	2.2	a	22.7	8.4	b	23.6	8.8	a	27.7	12.5	b	24.4	0.0	a
43.8	4.4	a	20.5	3.6	a	–	–	–	24.8	1.7	a(ε)	36.4	4.8	a	–	–	–
–	–	–	33.3	11.5	a	–	–	–	16.7	26.7	a	42.3	0.0	a	–	–	–
–	–	–	31.5	0.0	b	–	–	–	23.1	3.4	a	35.0	11.2	a	–	–	–
–	–	–	16.6	4.4	a	–	–	–	20.9	6.8	a	49.9	0.0	b	–	–	–
–	–	–	50.7	5.9	a	–	–	–	21.4	14.0	a	–	–	–	–	–	–
Mean 35.3	5.4		30.8	4.7		29.4	10.3		25.4	9.7		34.9	8.3		19.9	0.4	
SD 7.7	3.7		11.1	4.0		9.2	7.3		7.8	8.1		13.0	8.5		5.0	0.9	

[a] Orthogonal
[b] Parallel

Table 3 Mass balance calculation data for major elements involved in the retrograde reaction Car + Qtz → Chl + Phg2. Three different conditions are presented: *1* results obtained with measured volume change (%dV) and mineral proportions (%Chl) averaged for each sample (Table 2); *2* result obtained when adjusting mean mineral proportions (%Chl, in bold) so that ΔAl = 0; *3* result obtained when adjusting the mean volume change (%dV, in bold) so that ΔAl = 0. $\Delta\varsigma$ Overall charge of the reaction. Negative values correspond to minerals or elements effectively released

Molar mass balance constraints for reaction (1): Car (+Qtz) → Chl + Phg2

	Sample	Input volume proportions		Output minerals				Elements								
		%Chl	% dV	Car	Qtz	Chl	Phg	SiO_2aq[a]	Al	R^{2+}	NaK	H^+	O	$\Delta\varsigma$	(H_2O)	(H^+)
1-Measured	GV	35.30	5.40	5.30	1.35	−1.00	−2.74	−0.24	−0.20	−1.26	2.16	−7.72	−4.79	0.00	−4.31	0.97
	FBA	30.80	4.70	6.12	1.35	−1.00	−3.36	−0.23	0.12	−1.54	2.59	−9.74	−5.51	0.00	−5.05	0.12
	TPX	29.40	10.30	6.08	2.95	−1.00	−3.60	−0.83	0.04	−1.02	3.21	−9.14	−5.59	0.00	−3.93	−1.27
	COA	25.40	9.70	7.08	3.24	−1.00	−4.40	−0.70	0.23	−1.84	3.53	−11.53	−6.50	0.00	−5.09	−0.50
	JACQ	34.90	8.30	5.22	2.04	−1.00	−2.79	−0.75	−0.03	−0.43	2.41	−7.29	−4.76	0.00	−3.25	−1.43
	RFB	19.90	0.40	9.87	0.19	−1.00	−6.03	2.19	0.16	−5.34	4.37	−19.44	−8.78	0.00	−13.17	5.79
	Mean	29.28	6.47	6.61	1.85	−1.00	−3.82	−0.09	0.05	−1.91	3.05	−10.81	−5.99	0.00	−5.80	0.61
	SD	5.89	3.73	1.73	1.13	0.00	1.24	1.15	0.15	1.75	0.82	4.49	1.51	0.00	3.67	3.12
2-Iso-Al (%min)	Mean	30.25	6.47	6.26	1.77	−1.00	−3.54	−0.20	0.00	−1.60	2.83	−9.97	−5.67	0.00	−5.26	0.37
	SD	4.09	3.73	1.21	1.00	0.00	0.80	0.99	0.00	1.39	0.49	3.24	1.03	0.00	2.95	2.73
3-Iso-Al (%dV)	Mean	29.28	6.20	6.64	1.73	−1.00	−3.82	−0.02	0.00	−1.93	3.05	−10.92	−6.00	0.00	−5.96	0.81
	SD	5.89	3.87	1.79	1.14	0.00	1.24	1.22	0.00	1.79	0.82	−4.69	1.54	0.00	3.90	3.28

[a] The overall volume change associated with the reaction (%dV) is assumed to correspond to the volume of dissolved quartz (Qtz). Because not all silicon provided by the dissolved quartz is needed to balance the reaction, some silicon is generally released, probably as amorphous silica (SiO_2aq) – except for sample RFB. (H_2O) Moles of water released by the reaction, calculated from H^+ and O; (H^+) residual amount of H^+ not associated with oxygen

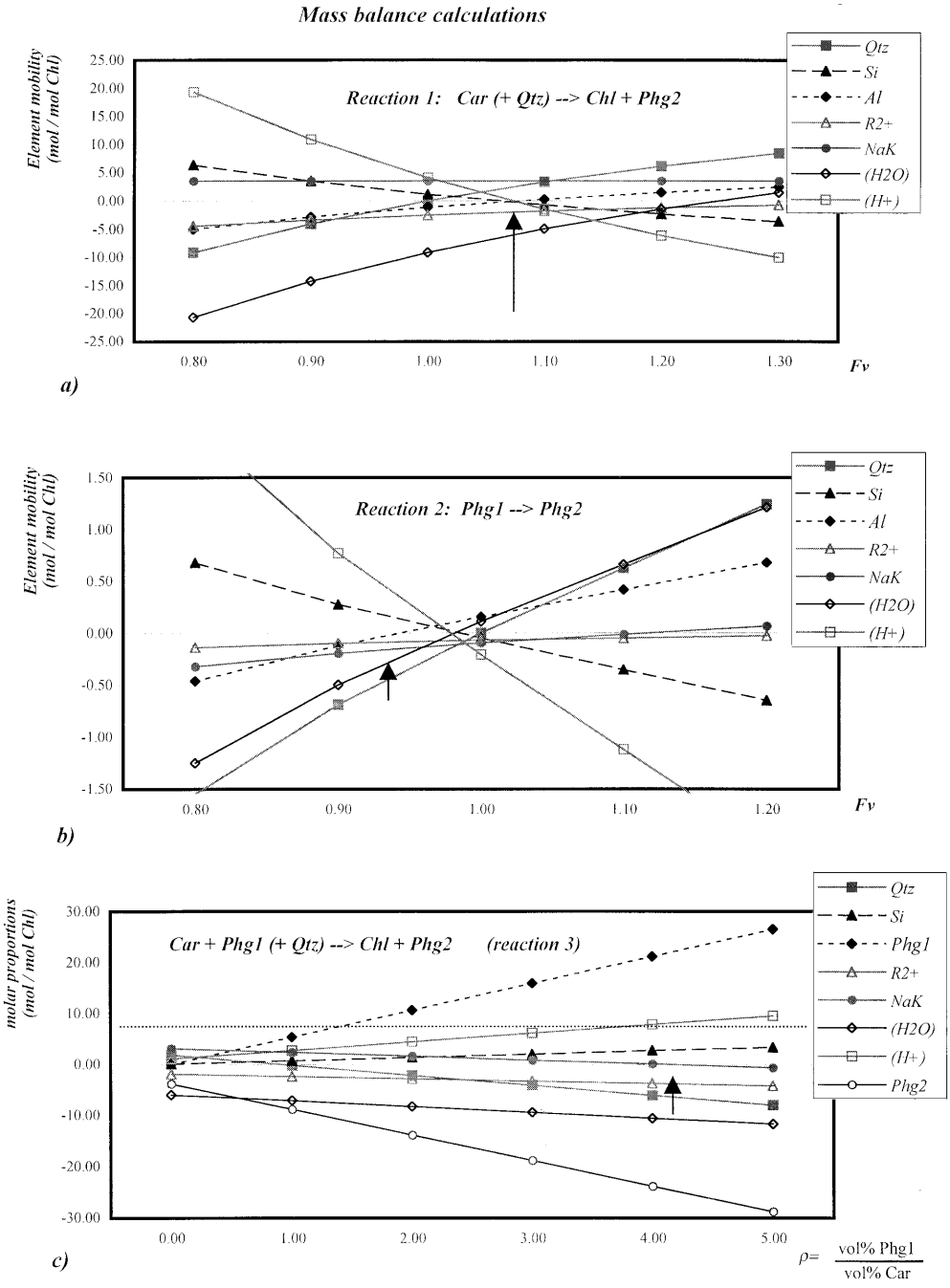

Fig. 9 **a** Gresens plot (Gresens 1967) showing the evolution of element mobility as a function of the volume factor Fv (= volume products/volume reactants) for the reaction Car + Qtz → Chl + Phg 2 (sample COA, Table 3 Negative values correspond to elements effectively released. See text. **b** Gresens plot showing the evolution of element mobility as a function of the volume factor Fv for the reaction Phg1 → Phg2 (sample COA, Tables 4 and 5). See text. **c** Plot showing element and mineral mobility when coupling reactions (1) and (2) for iso-aluminium conditions as a function of ρ (abscissa coordinate), that is the volume ratio of phengite to carpholite in a given outcrop under HP conditions. When $\rho \sim 4.3$ (*arrow*), the overall mass–balance reaction for the rock system is balanced for alkali elements and writes as reaction (3) (see text and Fig. 10a). *Horizontal dashed line* Moles of carpholite involved in the reaction

5. The iso-aluminium reference frame was here found to be a posteriori relevant to carpholite pseudomorphs – although the formation of carpholite-bearing or chlorite-bearing segregations clearly requires aluminium mobility. Because aluminium was claimed to be the least mobile element in many studies (e.g. Carmichael 1969; Kerrich 1990; Cesare 1994 for reviews), aluminium was often assumed to be immobile a priori and then used as a reference frame (e.g. Sicard-Lochon 1987). In our case, this type of assumption is only made for reactions involving phengite, for which no volume proportions are available (see below).

Evolution of phengite composition

The two phengite generations formed during the retrograde evolution (Phg1 and Phg2; see above), have distinct compositions – whereas that of chlorite remains constant in first approximation. It is thus possible to evaluate the transfer of elements required to form the latest Phg2 generation from pre-existing Phg1.

The balanced reaction obtained with the average composition of Phg1 and Phg2 from sample COA is given in Tables 4 and 5 (Fig. 9b, for the corresponding Gresens plot). To get an idea of the sensitivity of the

Table 4 Mass balance calculation data for major elements involved in the retrograde shift of phengite composition, expressed as Phg1 → Phg2, for different volume factor values (Fv; Gresens, 1967). Same abbreviations as in Table 3. Negative values correspond to minerals or elements effectively released. These calculations are made for 3 different phengite compositions (Table 5), which correspond to 1) Phg1 and Phg2 in a sample from Fraiteve (COA), 2) theoretical ideal compositions for phengite showing partial interlayer deficiency (Theor), 3) averaged compositions of Phg1 and Phg2 over the study area (SL). The three compositions do not lead to very different mass balance coefficients when compared for the case of iso-aluminium reactions (Fv ~ 0,94), (see text)

Molar mass balance constraints for reaction (2): Phg1 → Phg2 (+ Qtz)												
		Fv	Qtz	Si	Al	R^{2+}	NaK	O	H+	$\Delta\varsigma$	(H_2O)	(H^+)
1-Phg COA		0.80	−1.55	0.68	−0.46	−0.14	−0.32	0.10	−0.50	0.00	−1.25	2.00
		0.90	−0.69	0.27	−0.12	−0.10	−0.20	0.05	−0.22	0.00	−0.50	0.77
		1.00	0.00	−0.05	0.15	−0.07	−0.10	0.00	0.00	0.00	0.11	−0.21
		1.10	0.62	−0.35	0.41	−0.05	−0.02	−0.04	0.20	0.00	0.66	−1.12
		1.20	1.24	−0.65	0.68	−0.03	0.06	−0.08	0.40	0.00	1.21	−2.03
	Iso-Al	0.94	−0.39	0.13	0.00	−0.09	−0.15	0.03	−0.12	0.00	−0.23	0.33
2-Phg Theor		1.00	0.00	−0.10	0.20	−0.10	−0.10	0.00	0.00	0.00	0.20	−0.40
	Iso-Al	0.92	−0.52	0.14	0.00	−0.13	−0.18	0.03	−0.17	0.00	−0.25	0.34
3-Phg SL		1.00	0.00	−0.04	0.11	−0.08	−0.06	0.00	0.00	0.00	0.07	−0.14
	Iso-Al	0.96	−0.27	0.09	0.00	−0.09	−0.09	0.02	−0.09	0.00	−0.16	0.27

Table 5 Representative phengite compositions for the 3 different phengite used in the mass balance calculations (see Table 4). These phengite correspond to 1) Phg 1 and Phg 2 in a sample from Fraiteve (COA), 2) theoretical ideal compositions for phengite showing partial interlayer deficiency (Theor), 3) averaged compositions of Phg 1 and Phg 2 over the study area (SL; *: termed [B1] and [B2], respectively, in Agard et al. (2000a). Compositions for the first and third type correspond to electron microprobe analyses (see text for standards and procedure)

Structural formulae of phengite (on 11 oxygens)						
	COA		Theor		SL	
	Phg1	Phg2	Phg1	Phg2	Phg1[a]	Phg2[a]
Si	3.29	3.23	3.30	3.20	3.28	3.24
Ti	0.00	0.00	0.00	0.00	0.00	0.00
Al	2.46	2.62	2.40	2.60	2.50	2.61
Fe	0.09	0.07	0.10	0.07	0.10	0.05
Mn	0.00	0.00	0.00	0.00	0.00	0.00
Mg	0.18	0.14	0.20	0.13	0.16	0.13
Ca	0.00	0.00	0.00	0.00	0.00	0.00
Na	0.04	0.07	0.00	0.00	0.06	0.07
K	0.85	0.73	0.90	0.80	0.79	0.73

[a] Termed [B1] and [B2], respectively, in Agard et al. (2000)

mass balance estimates to slightly different Phg1 and Phg2 compositions, we also considered compositions averaged over the study area ('SL') and an ideal composition ('Theor'). These three different compositions are compared in the case of volume-for-volume reactions (Fv = 1, Table 4). For all three, some aluminium is needed and small amounts of silicon, alkali, and ferromagnesian elements are released. The Gresens plot for sample COA indicates that the overall element mobility is minimum for Fv, ~0.98–1 (Fig. 9b). However, contrary to carpholite pseudomorphs, we lack constraints on the bulk volume change of this reaction. If we assume for convenience that the reaction is iso-aluminium (see above discussion), then Fv = 0.94 and stoichiometric coefficients become:

$$\text{Phg1} + 0.13\ \text{SiO}_{2aq} + 0.33\ \text{H}^+ = 0.94\ \text{Phg2} + 0.39\ \text{Qtz} + 0.15\ \text{Alk}^+ 0.09\ \text{R}^{2+} + 0.23\ \text{H}_2\text{O} \quad (2)$$

In order to constrain the *overall* element mobility associated with the rock mineralogical changes, we may then combine reactions (1) and (2). If alkali are balanced between reactions (1) and (2) (this situation may arise when $\rho = \text{vol\%(Phg1)/vol\%(Car)} = 4.28$; see Fig. 9c and the discussion below), the following equation is obtained:

$$6.64\ \text{Car} + 21.55\ \text{Phg1} + 2.66\ \text{SiO}_{2aq} + 7.52\ \text{H}^+ = \text{Chl} + 24.15\ \text{Phg2} + 6.2\ \text{Qtz} + 3.76\ \text{R}^{2+} + 10.64\ \text{H}_2\text{O} \quad (3)$$

Discussion

Fluid composition in BS/GS segregations

All analysed inclusions are essentially aqueous. The absence of CO_2 in high-pressure inclusions is consistent with the occurrence of lawsonite, which is unstable in the presence of CO_2 (Nitsch 1972). Other gases, notably N_2, have been reported from high-pressure environments (e.g. Andersen et al. 1993), but they have not been encountered in the present study. This is in line with the very low amounts of additional volatile components found in carpholite-bearing metapelites from Creta (quadrupole mass spectrometry, Küster and Stöckhert 1997). Contrary to many alpine veins formed under greenschist-grade conditions (e.g. Poty et al. 1974), greenschist fluid inclusions are also devoid of significant amounts of CH_4 and CO_2. This may be because of the presence of disordered graphite (Goffé and Villey 1984; Beyssac et al. 1999) in the studied metapelites, which is known to buffer the fluid composition at nearly pure H_2O compositions for such P–T conditions (Connolly and Cesare 1993).

This aqueous fluid phase predominantly contains (Na, K)Cl salts, plus other dissolved species, which

slightly lower the temperature of initial melting (~−23.6 °C). Both BS and GS fluid inclusions show moderate salinities (< 15 wt% eq. NaCl), similar to those found in other BS metapelites (Giaramita and Sorensen 1994; Küster and Stoeckert 1997), but much less saline than inclusions in somewhat warmer BS settings (e.g. 30 wt% in the Cyclades; Barr 1990) or in many alpine eclogites (Philippot and Selverstone 1991; Philippot and Scambelluri 1995; Philippot et al. 1995).

A striking feature is that the salinities of the BS fluid inclusions are much more scattered than those of the GS fluid inclusions (Fig. 6). Fluid inclusions trapped at HP conditions ([Ia] and [Ib]) are more saline than the GS fluid inclusions. When comparing all fluid inclusions from the BS segregations, the successive generation of [Ia], [Ib] and then [Ic] inclusions (the latter also likely predate the generation of the GS fluids, as discussed below) reveals a trend of salinity decrease towards a nearly pure H_2O fluid phase.

Fluid source in GS segregations: HP mineral breakdown

The uniform salinity of the retrograde fluid phase and the abundance of GS segregations could be interpreted in terms of large amounts of pervasively circulating homogeneous fluids (e.g. Etheridge et al. 1983). However, infiltration of an externally derived exotic fluid (i.e. with a contrasted composition and/or isotopic signature) is unlikely, as shown by the results of Henry et al. (1996). Likewise, because GS segregations are not restricted to shear zones and generally not connected, large-scale (i.e. above the outcrop scale) fluid circulation in the SL unit itself was probably limited.

The alternative interpretation is to call for fluids locally released by the progressive breakdown of HP phases, notably carpholite (and lawsonite). Mass balance calculations show that the amount of water liberated during the retrograde evolution is large (0.9 mol H_2O per mol of retrogressed carpholite – reaction (1) – plus minor additional amounts of water released by phengite). Such a release of water-dominated fluids will result in a more dilute composition of the newly trapped fluid inclusions. If there is an interconnected porosity at the time this fluid is released, a uniform and dilute composition is to be expected.

The fluid composition represented by the GS inclusions could thus result from the mixing between two sources of fluid: (1) one initial and moderately saline fluid present during the prograde evolution (documented by [Ia] and [Ib] inclusions), and (2) a second nearly pure H_2O fluid that could be provided by the breakdown of carpholite.

The presence of almost pure H_2O [Ic] inclusions in the BS segregations may represent samples of this water-rich fluid released before equilibration with the adjacent pore fluid phase. Although it cannot be ascertained that [Ic] inclusions were trapped under HP conditions, their composition clearly differs from that of the GS inclusions ([Ir] and [Id]; Fig. 6). The variable salinities of the BS inclusions, which recall the scatter of salinities observed in alpine eclogites (Philippot and Selverstone 1991), support the existence of local equilibrium processes at HP conditions. But the decrease of salinity documented by the fluid inclusions from the BS segregations ([Ia] through [Ic]) could also partly reflect the progressive dilution of the fluid phase.

Quantitative estimates of fluid and element budget

Reactions (1) and (2) can be used to quantitatively evaluate the relevance of this hypothesis providing that (1) the average salinity for the BS fluid phase, (2) the value of the porosity and (3) the amount of carpholite and phengite (to estimate the amount of water liberated by a given volume of rock) are known. Fluid inclusion data suggest an average value of 10 wt% eq. NaCl for the BS fluid composition. The average porosity (Φ) for rocks equilibrated at conditions at ~10 kbar 350 °C can be extrapolated from the data of Bray and Karig (1985) on HP–LT Franciscan rocks and lies in the range 0.25–1 vol%. Carpholite and (HP) phengite may represent 20 vol%, each, of a given outcrop.

For each m^3 of rock containing 20 vol% of carpholite, 3.6×10^{-2} m^3 of water will be liberated through Reaction 1 (water density being close to 1 g cm^{-3} at the P–T conditions under consideration; e.g. Brown et al. 1989). Assuming $\Phi = 0.25$ vol%, this represents 15 times the amount of fluid present in the pore system, and the calculated GS fluid composition would amount to 0.6 wt% eq. NaCl. This is, however, a maximum estimate for the fluid release because carpholite often represents < 20 vol% of the host rock and because retrogression is not complete.

If we take an intermediate value for the porosity ($\Phi = 0.5$ vol%) and for carpholite (5–10 vol%), the dilution factor decreases and the final fluid composition lies in the range 2.5–4 wt% eq. NaCl, thus comparable with the measured average GS composition (3.7 wt% eq. NaCl). Fluid dilution generated through this process is thus significant. This shows that the internal fluid budget in the metapelites, in first approximation, may alone account for the evolution of the fluid salinity during the retrograde path.

We may now focus on the element budget necessary for the retrograde mineral evolution (that is, breakdown of carpholite, evolution of phengite composition and formation of quartz ± chlorite-bearing segregations). Large amounts of alkali are necessary [~0.5 mol per mol of carpholite, reaction (1)]. Yet, the evolution of phengite composition towards lower interlayer occupancy [reaction (2)] represents a significant source of alkali elements (with Phg1 = 10 vol%, this is ~11 times the amount present in a 10 wt% eq. NaCl fluid in a rock system with $\Phi = 0.5$ vol%).

Coupling reactions (1) and (2) (Gresens plot of Fig. 9c) shows that, whatever the value of the volume ratio 'ρ' = vol%(Phg1)/vol%(Car) (in a given outcrop

under HP conditions), iron, magnesium and water are always released and likely contribute to the deposition of GS veins in the pore system. However, phengite will only provide enough alkali to completely replace carpholite if $\rho \geq 4.3$ [$\rho = 4.28$, reaction (3)]. Hence, in order to totally replace 5% of the rock volume previously occupied by carpholite, 21.5% of the rock volume ought to be made of Phg1. This is equivalent, in terms of reaction products, to having 30 vol% of Phg2 in the rocks sampled, a fairly realistic situation (depicted in Fig. 10a).

On the other hand, the amount of phengite will clearly not be enough for large amounts of carpholite in a given outcrop (~20 vol%). The existence of localized relic accumulations of fresh carpholite, at the outcrop scale, and of partial pseudomorphs, at the thin section scale, may correspond to cases where the amount of phengite was a limiting factor.

Despite uncertainties (such as on the amount of BS or GS segregations), the above discussion on the magnitude of the element and fluid transfer in HP metapelites suggest that the retrograde mineralogical processes are locally balanced (for a rock with $\Phi = 0.5$ vol%, Car = 5 vol%, Phg1 = 21.5 vol% and a fluid salinity of 10 wt% eq. NaCl under HP conditions). Therefore, we propose that the retrograde fluid–mineral evolution may be viewed as a set of combined, complementary processes (in the sense of Carmichael 1969; Fig. 10b): (1) retrogression of HP minerals and adaptation of phengite (and chlorite) composition in the rock (1–1′; Fig. 10b), both in HP pseudomorphs and schist – alkali being predominantly provided by the high-pressure phengite; and (2) water release and element transfer (2–3–4; Fig. 10b) to form quartz (±chlorite) GS segregations in zones of enhanced-permeability (Yardley 1986).

Fig. 10 **a** Sketches depicting the evolution of the mineral proportions and of the fluid salinity for the model retrogression of a given rock volume (*square box*) initially containing 5 vol% of carpholite and 21.5 vol% of phengite under HP conditions ($\rho = 4.28$, Fig. 9c; Φ: porosity, in vol In this case, the evolution is locally buffered, both in terms of element (carpholite is completely pseudomorphed by chlorite and phengite) and fluids (salinity from 10 to 3 wt% eq. NaCl). See text. **b** Tentative model evolution of the rock system (at the metre scale) during the retrograde metamorphic history from blueschist (*BS*) to greenschist (*GS*) facies conditions, as deduced from fluid inclusion and mass transfer data. *Dashed white squares* show rock volumes (BS segregation + wallrock) where carpholite and quartz are replaced by chlorite and phengite during the retrograde evolution (*1* retrogression of HP minerals). At least some of the alkali elements necessary for this reaction are provided by phengite from the wallrock (*1′* adaptation of chlorite and mica composition in the rock). Water, iron and magnesium are transferred towards zones of enhanced-permeability to form GS segregations (*2* water release and element transfer; *3* formation of GS segregations; *4* possible migration along deformation-enhanced channelways). *Dotted arrows* Mass transfer of elements; *plain white arrows* sense of shear; *thick black line* shear band; *thin dark arrow* direction of extension and vein formation; *thin dark line* schistosity

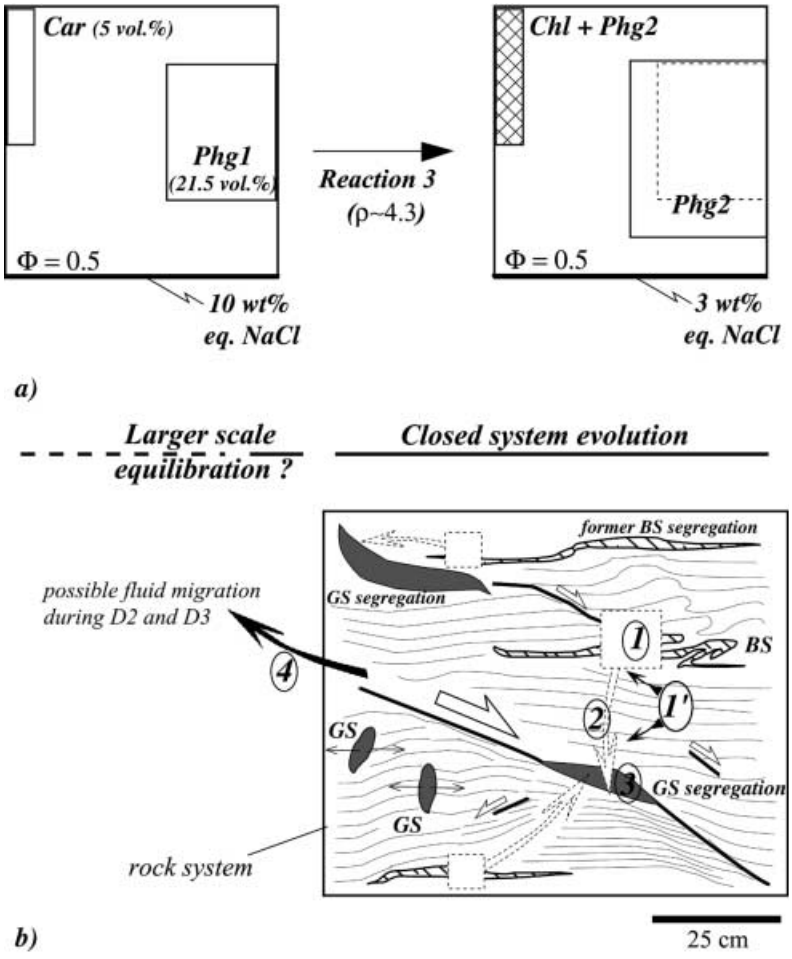

Conclusion

The combined study of fluid inclusions trapped in syn-metamorphic segregations and adjacent mineral reactions give some useful information on the fluid–rock interaction during the retrograde metamorphic evolution. The large amounts of water released by the destabilization of HP phases (notably carpholite) may account for (1) the dilution trend of the fluid phase with time recorded by the fluid inclusions from BS segregations, (2) the composition and constancy of the GS fluid inclusions, and (3) the large amount of GS segregations. Ferromagnesian elements released by the retrograde mineral reaction may contribute to the formation of chlorite-bearing quartz GS segregations.

Constraints on the rock–fluid (source and dilution) and element (alkali and ferromagnesian species) budget suggest that the rock system probably behaved as a closed system during the retrograde evolution. This result is compatible with the recognition by Henry et al. (1996) that no significant isotopic modification of the rock system occurred during the metamorphic evolution. It is also in line with the general opinion that large-scale circulation of fluids was limited in the case of the western Alps (Philippot and Scambelluri 1995) as opposed to subduction settings such as Santa Catalina Island (Bebout 1996).

This study underlines the high water retentivity of metapelites at high-pressure low-temperature conditions. It reveals that, at low temperature, an important water release can also occur during a cooling history linked to a considerable decrease of pressure. This water release should therefore have considerable effects on the properties of rocks and should be considered in the tectonic and geodynamic studies of HP–LT belts involving metapelites.

Acknowledgements We would like to thank E.A.J. Burke and L. André for access to the Raman facilities (Vrije University, Amsterdam) and to the laser ablation-coupled ICPMS facilities (University Libre de Bruxelles and Tervuren, Brussels), respectively. We thank B.W.D. Yardley and an anonymous reviewer for their constructive reviews, and P. Philippot for fruitful discussions at an earlier stage of this manuscript.

References

Agard P (1999) Evolution métamorphique et structurale des métapélites océaniques dans l'orogène Alpin: l'exemple des Schistes Lustrés des Alpes occidentales (Alpes Cottiennes), PhD Thesis, Univ PM Curie, Paris

Agard P, Goffé B (1998) Phengite buffering of mineral reactions in HP–LT metapelites. Mineral Mag 62A: 17–18

Agard P, Vidal O, Goffé B (2000a) Interlayer and Si content of phengite in HP–LT carpholite-bearing metapelites. J Metamorphic Geol (in press)

Agard P, Jolivet L, Goffé B (2000b) The Schistes lustrés complex: a key to understanding the exhumation of HP and UHP rocks in the Western Alps? Eclogae Geologicae Helvetiae (submitted)

Ague JJ (1991) Evidence for major mass transfer and volume strain during regional metamorphism of pelites. Geology 19: 855–858

Al-Khatib R, Touret JLR (1973) Fluides carboniques dans les roches du facies granulite du sud de la Norvège. Utilisation semi-quantitative de la surplatine à écrasement. Bull Soc Géol Fr 7: 321–325

Andersen T, Austrheim T, Burke EAT, Elvevold S (1993) N_2 and CO_2 in deep crustal fluids: evidence from the Caledonides of Norway. Chem Geol 108: 113–132

Austrheim H (1986) Eclogitization of lower crustal granulites by fluid migration through shear zones. Earth Planet Sci Lett 81: 221–232

Ballèvre M, Lagabrielle Y, Merle O (1990) Tertiary ductile normal faulting as a consequence of lithospheric stacking in the western Alps. Deep structure of the Alps. Mem Soc Géol Fr 156: 227–236

Banks DA, Yardley BWD (1992) Crush-leach analysis of fluid inclusions in small natural and synthetic samples. Geochem Cosmochim Acta 56: 245–248

Barfety JC, Lemoine M, Graciansky PC, Tricart P, Mercier D, with the collaboration of Pêcher A, Bertrand J, Nievergelt P, Amaudric du Chaffaut S, Dumont T, Monjuvent G, Goffé B, Kiénast JR, Mevel C, Gravost M, Sauret B, Godefroy P (1995) Notice explicative, Carte géol. France (1/50,000), feuille Briançon (823), Orléans

Barnicoat AC, Cartwright I (1995) Focused fluid flow during subduction: oxygen isotope data from high-pressure ophiolites of the western Alps. Earth Planet Sci Lett 132: 53–61

Barr H (1990) Preliminary fluid inclusion studies in a high-grade blueschist terrain, Syros, Greece. Mineral Mag 54: 159–168

Bebout GE (1996) Volatile transfer and recycling at convergent margins: mass-balance and insights from high-P/T metamorphic rocks. In: Bebout GE, Scholl DS, Kirby S, Platt JP (eds) Subduction: top to bottom. Geophys Monogr, Am Geophys Union, pp 179–193

Bebout G, Barton MD (1993) Metasomatism during subduction: products and possible paths in the Catalina schist, California. Chem Geol 108: 61–92

Belkin HE (1994) Microthermometric investigations: Th and Tm practical and theoretical aspects. In: De Vivo B, Frezzotti ML (eds) Fluid inclusions in minerals: methods and applications. IMA, Short course, Virginia Tech, Blacksburg, pp 7–23

Berman RG (1988) Internally-consistent thermodynamic data for minerals in the system Na_2O–K_2O–CaO–MgO–FeO–Fe_2O_3–Al_2O_3–SiO_2–TiO_2–H_2O–CO_2. J Petrol 29: 445–522

Berman RG, Perkins EH (1987) GEO-CALC: software for calculation and display of pressure–temperature-composition phase diagrams. Am Mineral 72: 861–862

Beyssac O, Goffé B, Rouzaud JN, Clinard C, Cassareuil J, Catel N (1999) From anthracite to graphite: influences of temperature, pressure and shear. In: Li BQ, Liu Z (eds) Prospects for coal science in the 21st century, vol 1. Shanxi Science and Technology Press, Taiyuan, P.R. China, pp 29–32

Bocquet J, Delaloye M, Hunziker JC, Krummenacher D (1974) K–Ar and Rb–Sr dating of blue amphiboles, micas and associated minerals from the Western Alps. Contrib Mineral Petrol 47: 7–26

Bousquet R, Goffé B, Henry P, Le Pichon X, Chopin C (1997) Kinematic, thermal and petrological model of the central Alps: lepontine metamorphism in the upper crust and eclogitisation of the lower crust. Tectonophysics 273: 105–127

Bray CJ, Karig DE (1985) Porosity of sediments in accretionary prisms and some implications for dewatering processes. J Geophys Res 90: 768–778

Brown PE, Lamb WM (1989) P–V–T properties of fluids in the system $H_2O \pm CO_2 \pm$ NaCl: new graphical presentations and implications for fluid inclusion studies. Geochem Cosmochim Acta 53: 1209–1221

Caby R, Kienast JR, Saliot P (1978) Structure, Métamorphisme et modèle d'évolution tectonique des Alpes Occidentales. Rev Géogr Phys Géol Dyn 20: 307–322

Carmichael DM (1969) On the mechanism of prograde metamorphic reactions in quartz-bearing pelitic rocks. Contrib Mineral Petrol 20: 244–267

Caron JM (1974) Rapports entre diverses 'générations' de lawsonite et les déformations dans les 'Schistes lustrés' des Alpes cottiennes septentrionales (France et Italie). Bull Soc Géol Fr 16: 255–268

Caron JM (1977) Lithostratigraphie et tectoniqe des 'Schistes lustrés' dans les alpes cottiennes septentrionales et en Corse orientate. Ph-D thesis, Univ Louis Pasteur, Strasbourg

Cesare B (1994) Synmetamorphic veining: origin of andalusite-bearing veins in the Vedrette de Ries contact aureole, Eastern Alps, Italy. J Metamorph Geol 12: 643–653

Chopin C, Schreyer W (1983) Magnesiocarpholite and magnesiochloritoid: two index minerals of pelitic blueschists and their preliminary phase relations in the model system MgO–Al_2O_3–SiO_2–H_2O. Am J Sci 280-A: 72–96

Chopin C, Henry C, Michard A (1991) Geology and petrology of the coesite-bearing terrain, Dora Maira massif, Western Alps. Eur J Mineral 3: 263–291

Connolly JAD, Cesare B (1993) C–O–H–S fluid composition and oxygen fugacity in graphitic metapelites. J Metamorph Geol 11: 379–388

Crawford ML, Hollister LS (1986) Metamorphic fluids: the evidence from fluid inclusions. In: Walther JV, Wood BJ (eds) Fluid–rock interactions during metamorphism. Advances in physical geochemistry. Springer, Berlin Heidelberg New York, pp 1–35

De Vivo B, Frezzotti ML (1994) Fluid inclusions in minerals: methods and applications. Virginia Tech, Blacksburg

Deville M, Fudral S, Lagabrielle Y, Marthaler M, Sartori M (1992) From oceanic closure to continental collision: a synthesis of the 'Schistes Lustrés' metamorphic complex of the Western Alps. Geol Soc Am Bull 104: 127–139

Etheridge MA, Wall VJ, Vernon RH (1983) The role of the fluid phase during regional metamorphism and deformation. J Metamorph Geol 1: 205–226

Evans BW (1990) Phase relations of epidote-blueschists. Lithos 25: 3–23

Ferry JM (1994) A historical review of metamorphic fluid flow. J Geophys Res 99: 15487–15498

Fyfe WS, Price NJ, Thompson AB (1978) Fluids in the Earth's crust: developments in geochemistry. Elsevier, Amsterdam, p 390

Getty SR, Selverstone J (1994) Stable isotopic and trace element evidence for restricted fluid migration in 2 GPa eclogites. J Metamorph Geol 12: 747–760

Giaramita MJ, Sorensen SS (1994) Primary fluids in low-temperature eclogites: evidence from two subduction complexes (Dominican Republic, and California, USA). Contrib Mineral Petrol 117: 279–292

Gillet P, Goffé B (1988) On the significance of aragonite occurrences in the Western Alps. Contrib Mineral Petrol 99: 70–81

Goffé B (1982) Définition du faciès à Fe–Mg carpholite–chloritoide, un marqueur du métamorphisme de HP-BT dans les métasédiments alumineux, Ph-D thesis, Univ PM Curie, Paris

Goffé B, Bousquet R (1997) Ferrocarpholite, chlorito et lawsonite dans les métapelites des unités du Versoyen et du Petit St Bernard (zone valaisanne). Schweiz Mineral Petr Mitt 77: 137–147

Goffé B, Chopin C (1986) High-pressure metamorphism in the Western Alps: zoneography of metapelites, chronology and consequences. Schweiz Mineral Petr Mitt 66: 41–52

Goffé B, Villey M (1984) Texture d'un matériel carboné impliqué dans un métamorphisme haute pression-basse température (Alpes françaises). Les hautes pressions influencent-elles la carbonification? Bull Minéral 107: 81–91

Goffé B, Murphy WM, Lagache M (1987) Experimental transport of Si, Al and Mg in hydrothermal solutions: an application to vein mineralization during high-pressure, low-temperature metamorphism in the French Alps. Contrib Mineral Petrol 97: 438–450

Gratier JP, Jenatton L (1984) Deformation by solution–deposition, and re-equilibration of fluid inclusions in crystals depending on temperature, internal pressure and stress. J Struct Geol 6: 189–200

Gresens RL (1967) Composition–volume relationships of metasomatism. Chem Geol 2: 47–65

Henry C, Burkhard M, Goffé B (1996) Evolution of synmetamorphic veins and their wallrocks through a Western Alps transect: no evidence for large-scale fluid flow! Chem Geol 127: 81–109

Henry P, Le Pichon X, Goffé B (1997) Kinematic, thermal and petrological model of the Himalayas: constraints related to metamorphism within the underthrust Indian crust and topographic elevation. Tectonophysics 273: 31–56

Jamveit B, Yardley BWD (1997) Fluid flow and transport in rocks. Chapman and Hall, London

Kerrick DM (1990) The Al_2SiO_5 polymorphs. Rev Mineral, Mineral Soc Am, vol 22, p 406

Küster M, Stöckert B (1997) Density changes of fluid inclusions in high-pressure low-temperature metamorphic rocks from Crete: a thermobarometric approach on the creep strength of the host minerals. Lithos 41: 151–167

Lagabrielle Y (1987) Les ophiolites: marqueurs de l'histoire tectonique des domaines océaniques. Thesis, Univ de Bretagne, Brest

Le Pichon X, Bergerat F, Roulet MJ (1988) Plate kinematics and tectonics leading to the Alpine belt formation; a new analysis. Geol Soc Am 218: 111–131

Lemoine M, Bas T, Arnaud-Vanneau A, Arnaud H, Dumont T, Gidon M, Bourbon M, De Graciansky PC, Rudkiewicz JL, Megard-Galli J, Tricart P (1986) The continental margin of the Mesozoic Tethys in the Western Alps. Mar Petrol Geol 3: 179–199

Liewig N (1981) Les phengites: marqueurs géométriques, chimiques et isotopiques de l'histoire des roches métamorphiques. Application aux Schistes lustrés des Alpes Cottiennes. Thesis, Université Louis Pasteur, Strasbourg

Liu ML, Yund RA (1993) Transformation kinetic of polycrystalline aragonite to calcite: new experimental data, modelling, and implications. Contrib Mineral Petrol 114: 465–478

Mandelbrot B (1977) The fractal geometry of nature. Freeman, San Francisco

Massonne HJ (1995) Experimental and petrogenetic study of UHPM. In: Coleman RG, Wang X (eds) Ultrahigh-pressure metamorphism. Cambridge University Press, Cambridge, pp 33–95

Michard A, Goffé B, Chopin C, Henry C (1996) Did the Western Alps develop through an Oman-type stage? The geotectonic setting of high-pressure metamorphism in two contrasting Tethyan transects. Ecol Geol Helv 89: 43–80

Moree M (1998) The behaviour of retrograde fluids in high-pressure settings. PhD Thesis, Vrije Univ, Amsterdam

Mullis L, Dubessy J, Poty B, O'Neil J (1994) Fluid regimes during late stages of a continental collision: physical, chemical, and stable isotope measurements of fluid inclusions in fissure quartz from a geotraverse through the central Alps, Switzerland. Geochem Cosmochim Acta 58: 2239–2267

Nitseli KH (1972) The P–T–XCO_2 stability field of lawsonite. Contrib Mineral Petrol 34: 116–134

Oberhänsli R, Goffé B, Bousquet R (1995) Record of a HP–LT metamorphic evolution in the Valais zone. In: Lombardo B (ed) Studies on metamorphic rocks and minerals of the Western Alps, Suppl Boll Mus Reg Sci Nat 13: 221–239

Oliver NHS (1996) Review and classification of structural controls on fluid flow during regional metamorphism. J Metamorph Geol 14: 477–492

Philippot P (1990) Opposite vergence of nappes and crustal extension in the French-Italian Western Alps. Tectonics 9: 1143–1164

Philippot P, Scambelluri M (1995) The composition and behaviour of fluids in high-pressure rocks from the Alps: a review. In: Lombardo B (ed) Studies on metamorphic rocks and minerals of the Western Alps, Suppl Boll Mus Reg Sci Nat 13: 75–99

Philippot P, Selverstone J (1991) Trace-element-rich brines in eclogitic veins: implications for fluid composition and transport during subduction. Contrib Mineral Petrol 106: 417–430

Philippot P, Chevallier P, Chopin C, Dubessy J (1995) Fluid composition and evolution in coesite-bearing rocks (Dora-Maira massif, Western Alps): its implications for element recycling during subduction. Contrib Mineral Petrol 121: 29–44

Platt JP, Behrmann JH, Cunningham PC, Dewey JF, Helman M, Parish M, Shepley MG, Wallis S, Weston PJ (1989) Kinematics of the alpine arc and the motion history of Adria. Nature 337: 158–161

Pognante U (1991) Petrological constraints on the eclogite- and blueschist-facies metamorphism and P–T-t paths in the Western Alps. J Metamorph Geol 9: 5–17

Poty BP, Stalder HA, Weisbrod AM (1974) Fluid inclusions studies in quartz from fissures of Western and Central Alps. Schweiz Mineral Petr Mitt 54: 717–752

Ramsay JG (1980) The crack-seal mechanism of rock deformation. Nature 284: 135–139

Ramsay JG, Huber MI (1983) Modern structural geology, vol 1: strain analysis. Academic Press, London

Reynolds SJ, Lister GS (1987) Structural aspects of fluid–rock interactions in detachment zones. Geology 15: 362–366

Roedder E (1984) Fluid inclusions, Rev Miner, Mineral Soc Am, vol 14, p 644

Rumble D (1994) Water circulation in metamorphism. J Geophys Res 99: 15499–15502

Saliot P (1978) Le métamorphisme dans les Alpes françaises. Ph-D thesis, Univ PM Curie, Paris

Saliot P, Dal Piaz GV, Frey M (1980) Métamorphisme de haute-pression dans les Alpes franco-italo-suisses. Géol Alp 56: 203–215

Selverstone J, Morteani G, Staude JM (1991) Fluid channelling during ductile shearing: transformation of granodiorite into aluminous schist in the Tauern Window, Eastern Alps. J Metamorph Geol 9: 419–431

Selverstone J, Franz G, Thomas S (1992) Fluid heterogeneities in 2 GPa eclogites: implications for element recycling during subduction. Contrib Mineral Petrol 112: 341–357

Shepherd TJ, Rankin Aff, Alderton DHM (1985) A practical guide to fluid inclusion studies. Blackie, London

Sicard-Lochon E (1987) La lawsonite et ses pseudomorphoses. PhD Thesis, Univ Claude Bernard-Lyon I

Spear FS (1993) Metamorphic phase equilibria and pressure–temperature-time paths. Min Soc Am Monogr, Washington, p 799

Stampfli GM, Marchant RH (1997) Geodynamic evolution of the Tethyan margins of the Western Alps. In: Pfiffner OA, et al (eds) Deep structure of the Swiss Alps: results of NRP-20, Birkhauser, Basel, pp 223–239

Sterner SM, Hall DL, Keppler H (1995) Compositional re-equilibration of fluid inclusions in quartz. Contrib Mineral Petrol 119: 1–15

Takeshita H, Shimoya H, Itaya T (1994) White mica K–Ar ages of blueschist-facies rocks from the Piemonte 'cale-schists' of the Western Alps. Island Arc 3: 151–162

Touret JLR (1977) The significance of fluid inclusions in metamorphic rocks. In: Fraser CDG (ed) Thermodynamics in geology. Dordrecht, Boston, pp 203–217

Touret JLR (1981) Fluid inclusions in high-grade metamorphic rocks. In: Hollister LS, Crawford ML (eds) Short-course in fluid inclusions: applications to petrology. Min Assoc Can, vol 6, pp 182–208

Touret JLR (1992) Fluid inclusions in subducted rocks. Proc Kon Ned Akad Wetensch 95: 385–403

Touret JLR (1996) Lile depletion in granulites: myth or reality. In: Demaiffe D (ed) Petrology and geochemistry of magmatic suites in the continental and oceanic crusts: a volume dedicated to Prof. J. Michot, Univ Libre Bruxelles et Tervuren, Royal Museum Central Africa, pp 53–72

Tricart P (1980) Tectoniques superposées dans les Alpes occidentales au sud du Pelvoux. Evolution structurale d'une chaîne de collision. Ph-D thesis, Univ Louis Pasteur, Strasbourg

Vidal O, Theye T (1996) Petrology of Fe–Mg-carpholite-bearing metasediments from NE Oman; discussion. J Metamorph Geol 14: 381–397

Vidal O, Theye T, Goffé B (1992) Experimental study of the stability of sudoite and magnesiocarpholite and calculation of a new petrogenetic grid for the system FeO–MgO–Al_2O_3–SiO_2–H_2O. J Metamorph Geol 10: 603–614

Vidal O, Goffé B, Bousquet R, Parra T (1999) An empirical chloritoid–chlorite Mg–Fe exchange thermometer and thermodynamic data for daphnite. J Metamorph Geol 17: 25–40

Vityk MO, Bodnar RJ, Schmidt CS (1994) Fluid inclusions as tectonothermobarometers: relation between pressure–temperature history and reequilibration morphology during crustal thickening. Geology 22: 731–734

Walther JV, Wood BJ (1986) Fluid–rock interactions during metamorphism. Springer, Berlin Heidelberg New York

Yardley BD (1986) Fluid migration and veining in the Connemara schists Ireland. In: Walther JV, Wood BJ (eds) Fluid–rock interactions during metamorphism. Springer, Berlin Heidelberg New York, pp 109–131